Monitoring winter wheat crop traits change during crop development using Sentinel-1 backscatters.

Abstract

It is important for farmers to monitor the development changes in winter wheat (*Triticum aestivum* L.) crop structure to assess plant response to crop management and environmental changes. Even in cloudy conditions, radar satellite imagery has the potential to provide near real-time and reliable information about crop development that surpasses optical satellite imagery. In this study, Sentinel-1A/1B backscattering parameters for co-polarization (VV), cross-polarization (VH), differences of dual polarizations (VH-VV), and combination of dual polarizations (VH+VV) were evaluated to estimate changes in shoot density (SD), green area index (GAI), aboveground dry biomass (AGDB), plant height (PH), and leaf nitrogen content (LNC) throughout the winter wheat growing season. In order to eliminate noise caused by inverse scattering, local weighted scatterplot smoothing (LOWESS) was applied to backscatter parameters during post-processing. The correlation of backscatter parameters to the in-situ winter wheat plant traits in the fields were assessed in the Republic of Ireland and the United Kingdom over two crop growing cycles. The Sentinel-1 backscatter parameters were correlated to SD, GAI, AGDB, PH, and LNC using Support Vector Regression (SVR), Random Forest Regression (RFR), and K-Nearest Neighbors Regression (KNNR). The results presented good prediction of GAI, AGDB, PH, and LNC were possible with R^2 between 0.72 to 0.95 when modelled using datasets from specific growth stages indicative of morphological

changes in plant and R^2 between 0.69 to 0.94 when modelled using datasets from full growth stages. It was concluded that it would be possible to develop continuous monitoring of winter wheat throughout the growing season that would not be influenced by cloud cover. Subsequent work will examine the best way to use these data for optimum crop husbandry.

Keywords: Machine Learning, Radar Backscatter, Precision Agriculture, Crop Monitoring, Remote Sensing.

1. Introduction

Development of winter wheat occurs over a series of morphological stages that culminate at maturity and harvest of the grain crop. Optimum plant husbandry requires knowledge of current crop conditions during each growth stage. For the application of plant growth regulators, it is important to observe changes in plant morphological characteristics so as to prevent crop damage and improve crop growth (Nasir et al., 2019; Voronov et al., 2021). Moreover, the morphological characteristics of plants also serve as indicators of plant response to environmental conditions (Lopez Laphitz et al., 2016; Bano et al., 2019). To ensure optimum yield and return on investment during the harvest season, farmers must estimate crop traits accurately and in a timely manner. This valuable information about crop conditions and variation in plant morphology, allows them to respond precisely and specifically to problems as they arise (Veloso et al., 2017).

In agriculture, remote sensing technology is widely used for monitoring and studying crop growth status and forecasting crop production (Atzberger, 2013). Radar spaceborne images could play a more important role in agriculture because when compared to optical spaceborne images for monitoring crop growth, they can be used during cloudy conditions and during the absence of sunlight (Liu et al., 2019). In addition, the backscatter is sensitive to the surface dielectric constant and plant geometry, enhancing its potential for application in agriculture crop monitoring (McDonald et al., 1999; Macelloni et al., 2001).

With the availability of Copernicus Sentinel-1A and 1B satellite, the frequency of the image availability increased to 1.5 - 4 days for the Republic of Ireland (IE), 1.5 -3 days for the United Kingdom (UK), and 6 days for other regions outside the Europe region. The Sentinel-1 C-band Synthetic-Aperture-Radar (SAR) instrument can collect images with spatial resolution up to 5m x 5m in StripMap mode with swaths of up to four kilometers wide. Plant traits are highly variable phenomena in time and space. Sentinel-1 has a high spatial-temporal resolution and active C-band observations that are sensitive to vegetation dynamics, making it an excellent option for monitoring crops at the field and regional scales (Monsivais-Huertero et al., 2020).

Sentinel-1 satellite images have been utilized in many studies to monitor the growth in biomass of winter wheat (Kumar et al., 2018), green area index (Veloso et al., 2017), leaf area index (Ouaadi et al., 2021), plant height (Kumar et al., 2018), crop water content (Han et al., 2019), and phenology (Schlund & Erasmi, 2020). However, all these studies have used a relatively small study area and only involved single or few orbit passes images which can bypass the backscatter bias due to incidence angle difference and geometry effects (Arias et al., 2022). Gorrab et al., (2021) reported that no impact of using

2 orbit passes and incidence angles in estimating winter wheat vegetation variables in their experiment. Their experiment also compared VV, VH, VH+VV, and VH-VV backscatter with cumulative values and found out that the cumulative backscatter of VH+VV best estimated wheat height (R^2=0.89) and total dry mass (R^2=0.74). Cumulative backscatter of VV gave the best estimation of total fresh mass (R^2=0.51) and cumulative backscatter of VH gave the best estimation of water content (R^2=0.47). It was, however, necessary to calibrate the model using imagery acquired in multiple orbital directions and at a wide range of incidence angles to model the large study area beyond a single orbit pass or narrow range of incidence angles.

The objective of the work reported here was to establish the feasibility of developing a winter wheat growth monitoring method covering a wide geographical area using Sentinel-1 images, particularly with different incidence angles, varying in orbit directions and multiple orbits passes to achieve high spatial-temporal resolution. This research builds on the work of (Goh et al., 2022) to enhance the performance of existing winter wheat growth monitoring models using Sentinel-2 especially the temporal resolution to identify winter wheat underperformance growth zone.

The research, (1) implemented data reduction using a backscatter smoothing algorithm at post-processing (2) analyzed the trend of winter wheat plant traits over different growth stages. (3) investigated the potential of Sentinel-1 VV, VH, VH-VV, and VH+VV backscattering parameters to estimate SD, GAI, AGDB, PH, and LNC using a multivariate supervised machine learning approach RFR, SVR, and KNNR and, (4) compared the modeling of complete growth stages, specific growth stages of plant morphological

changes, and primary growth stages to determine the prediction power of Sentinel-1 backscatters to the changes to plant morphology.

2. Materials

2.1 Study Area

The study area (*Fig.1)* covered two countries, IE and the UK, including 75 winter wheat fields over a geodesic measurement with an east-west length of approximately 640 km and a north-south length of approximately 300 km. The field sizes sampled ranged from 2 ha to 76 ha, which correspond to the recommended field size for retrieving biophysical parameters from Sentinel-1 data using calculation in Patel & Srivastava, (2013). All winter wheat fields were relatively flat. The annual weather data for the sampling period are detailed in (*Table 1*). The soil texture ranged from clay loam to loam in IE, from clay loam to silt loam in the northern and eastern UK, clay loam to loam in the western UK, silt loam, and chalky in the southern UK.

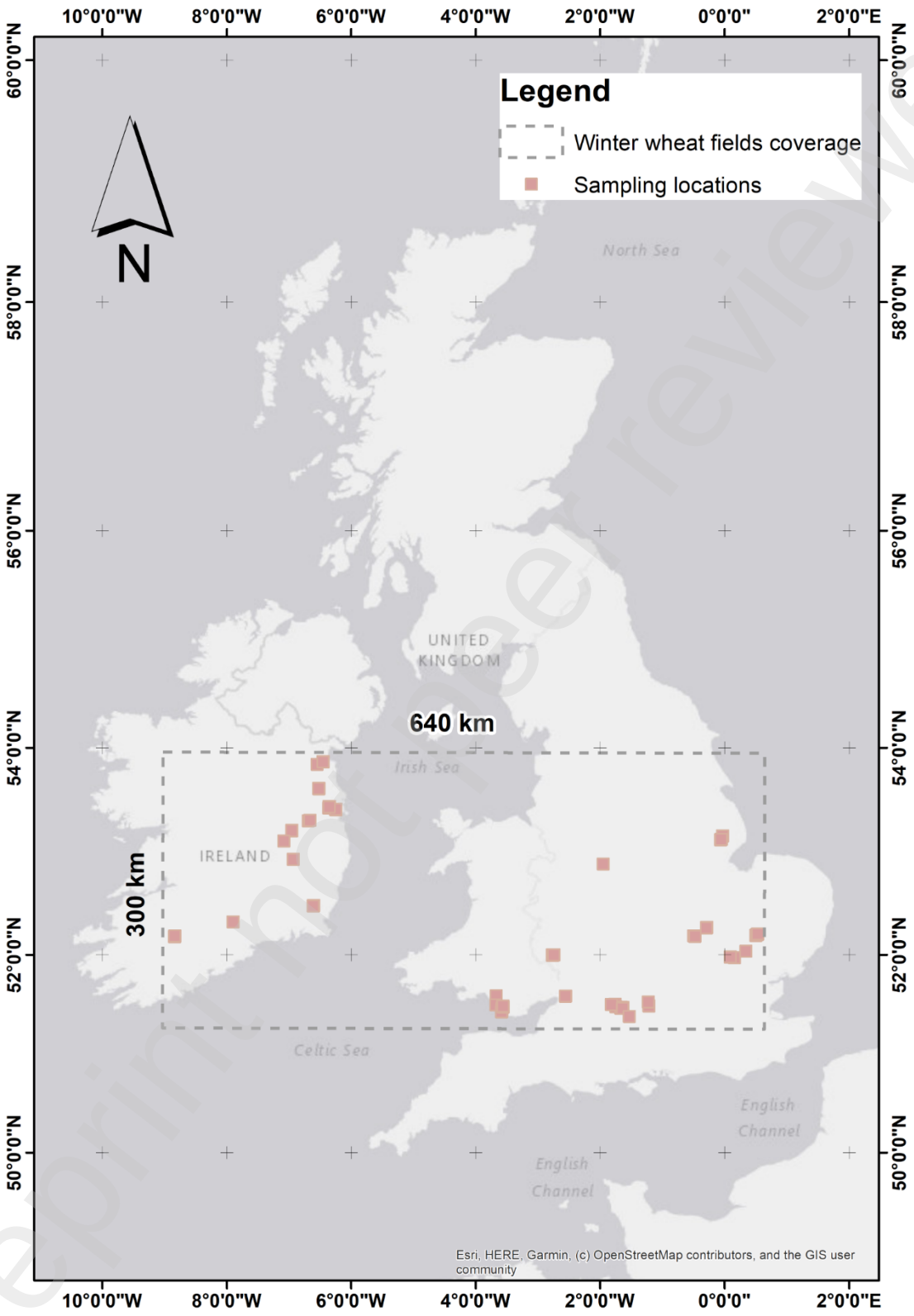

Fig.1: Location of study sites across the Republic of Ireland (IE) and the United Kingdom (UK)

Table 1: Annual mean temperature, rainfall, and sunshine across IE and UK in 2020 and 2021

Country	Year	Mean Temperature	Mean Rainfall	Mean Sunshine
IE	2020	10.0 º C	1400 mm	1446 hours
IE	2021	10.4 º C	1196 mm	1412 hours
UK	2020	9.6 º C	1308 mm	1495 hours
UK	2021	9.3 º C	1077 mm	1391 hours

Note. The weather data for IE in 2020 and 2021 are from the Climatology and Observations Division of Met Eireann, (https://www.met.ie/climate/past-weather-statements). The data for the UK in 2020 and 2021 are from the national meteorological service for the UK, (https://www.metoffice.gov.uk/research/climate/maps-and-data/summaries/index).

2.2 In-situ Data Measurement

The winter wheat was sown in the study area between September and December and harvested between the end of July and August. In-situ data are essential for the analysis of the Sentinel-1 backscatter in relation to the actual crop condition on the ground. During the winter wheat crop development period in 2020 and 2021, 75 fields were sampled on dates to characterize four major growth stages of winter wheat namely tillering, stem elongation, heading and flowering, and fruiting, The in-field growth stages were estimated using a growing degree days calculator and further confirmed by the farmers before visiting the field for crop sampling. The growth stages in this study were described using the BBCH scale (named after Biologische Bundesanstalt, Bundessortenamt, und CHemische Industrie) (Meier et al., 2009). Each field was sampled using five 0.5m x 0.5m quadrats. Quadrats were randomly located about 15m apart and at least 20m from the nearest field boundary to avoid the edge effect. The total samples size was 1500. The

actual growth stage was recorded by observing the plant morphology of each quadrat and matching the BBCH scale description. Four crop biophysical variables namely, SD, GAI, PH, and Leaf Nitrogen Concentration (LC%) were measured within quadrat. Four more sampling locations were selected randomly with each approximately 15-20m apart. Above-ground fresh biomass (AGFB), AGDB, Leaf dry biomass (LDB) and plant water content (PWC), and LNC were subsequently determined in the laboratory. Other than crop biophysical variables, quadrat coordinates (latitude and longitude), sample photos for each quadrat, and farmer field observation notes were recorded. The in-situ data measurement methods are described in *(Table 2).*

Table 2: Measurements method of in-situ data during winter wheat crop development period in 2020 and 2021.

In Situ Data	Method
Quadrat location	Latitude and Longitude to nearest 0.00001 degrees
Growth Stage (GS)	Plant morphology of each quadrat was matched with the BBCH scale description and the specific BBCH code was recorded. Growth stage based on BBCH scale
Shoots Density (SD)	Total count of shoots per quadrat.
Green Area Index (GAI)	The ratio of green leaf and stem area to the area of ground, an average of three measurements from BASF GAI smartphone application per quadrat.
Plant Height (PH)	Average of three above-ground plant height measurements per quadrat using self-retracting metal tape.

Leaf N Concentration (LC%)	Average of ten readings measured by SPAD-502Plus chlorophyll meter from uppermost leaves per quadrat. Calculate the final value using Eq.1 from (KONICA MINOLTA, 2009) LC% = 0.079(SPAD value) -0.154 Eq. 1
Aboveground Fresh Biomass (AGFB)	Destructive sampling of fresh plants per quadrat. The fresh plants were weighed using a digital weighing scale with a maximum capacity of 5000g to obtain AGFB. The fresh plant was further split into leaves, stems, and spikes.
Aboveground Dry Biomass (AGDB)	The total weight of oven-dried leaves, stems, and spikes (dried in the oven at 70 ºC for 48 hours until constant weight) were obtained respectively and also added up to calculate the total aboveground dry biomass.
Leaf Dry Biomass (LDB)	Weight of oven-dried plant leaves per quadrat.
Plant Water Content (PWC)	Subtraction of Aboveground Fresh Biomass and Aboveground Dry Biomass.
Leaf Nitrogen Content (LNC)	Value of Leaf N Concentration multiplies with the Leaf Dry Biomass using Eq.2 to get Leaf N Content (Li et al., 2018). LNC=LDB x LC% Eq. 2

2.3 Sentinel-1 Images

Sentinel-1A and Sentinel-1B Level-1 Ground Range Detected (GRD) images from 1st March to 30th June 2020 and 1st March to 30th June 2021 were acquired for the 75 winter wheat fields. The GRD scenes consist of dual band cross-polarization, vertical transmission (VV), and horizontal reception (VH). The pre-processing of each scene was done using Sentinel-1 toolbox's functions as follows, (1) apply an orbit file (2) GRD border noise removal (3) thermal noise removal (4) radiometric calibration (5) terrain flattening

(6) terrain correction using SRTM 30-meter DEM, resample pixel spacing to 10m spatial resolution (7) subset to the winter wheat field boundary (8) convert backscatter coefficient (σ°) to decibels (dB) using log scaling. Each Sentinel-1 images corresponded to one of nine orbit passes with incidence angles ranging from 30.28º - 45.27º are shown in *(Fig. 2).*

Fig. 2: All Sentinel-1 images corresponded to multiple orbit passes, different orbit directions, and multiple incidence angles acquired for the study fields in IE and UK. ASC stands for "Ascending" and DSC stands for "Descending".

3. Methods

3.1 Backscatter post-processing using data reduction algorithm.

There is radiometric uncertainty or noise in the Sentinel-1 backscatter due to the calibration of Sentinel-1A and 1B (Schwerdt et al., 2017), variations in multiple orbit passes and incidence angles (Kaplan et al., 2021), surface roughness (Anderson & Croft, 2009), dielectric constant (crop canopy water, soil moisture, dew, and precipitation) (Khabbazan et al., 2019), geometric arrangement (Yan et al., 2018), or frozen soil (Baghdadi et al., 2018). However, these factors are not fully understood in different parts of the world and are not always reproduced by other experiments or backscattering models. Thus, we performed a data reduction method, using a locally weighted scatterplot smoothing (LOWESS) algorithm for noise reduction of radiometric uncertainty across phenology stages within a wide geographical extent.

The algorithm was used in many applications for noise reduction in remote sensing derived values (Derkacheva et al., 2020; Zhang et al., 2022). LOWESS was developed by Cleveland, (1979). It is a method of fitting a linear or quadratic function to data points that is least squared distance from them. The amount of subset data points is defined for each weighted least square using the span parameter which is between 0 and 1. The optimal span number is depending on the total number of data points for smoothing variance trends and can be obtained using `chooseLowessSpan` function in R package (R Core Team, 2022).

In this research, the backscatters extracted from FlaxClose field in dense time series (*Fig. 3a-d)* show the fluctuation trend over the growing period using all available Sentinel-1

imagery with multiple incidence angles and orbit passes. In contrast, (*Fig. 3e-h*) presents the backscatters time series classified by four different incidence angle and orbit pass. By splitting the backscatter based on single incidence angle and orbit pass, the trends significantly less fluctuation over the growing season. The VH polarizations in (*Fig. 3e)* illustrates the influence of incidence angle reduced through application of terrain flattening to normalize the incidence angle of the Sentinel-1 imagery. However, the VV polarization in (*Fig. 3f*) shows the influence of the incidence angle remains. This finding is consistent with the finding of (Arias et al., 2022). The LOWESS was applied to the VH, VV, VH-VV and VH+VV backscatters parameter (*Fig. 3i-l*) to improve and reveal a better trend to describe the winter wheat growth. This method was replicated to the rest of 74 winter wheat fields.

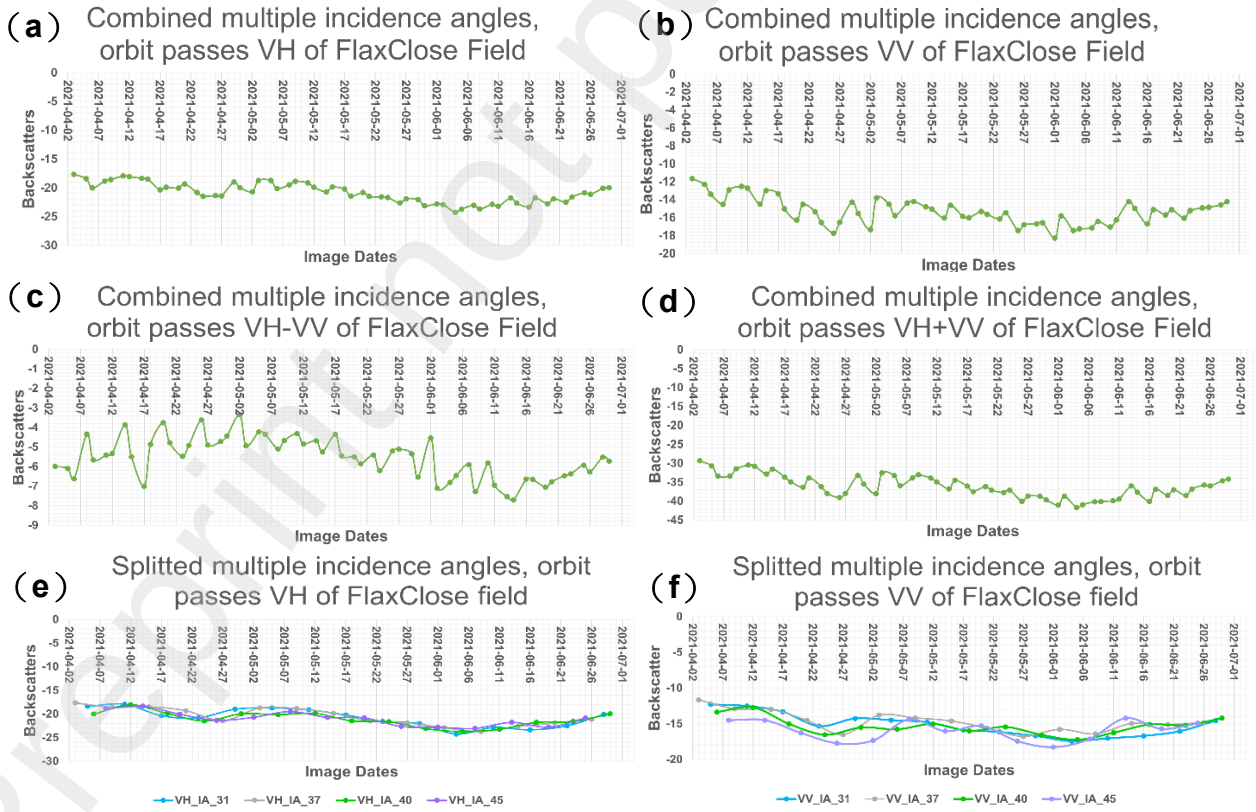

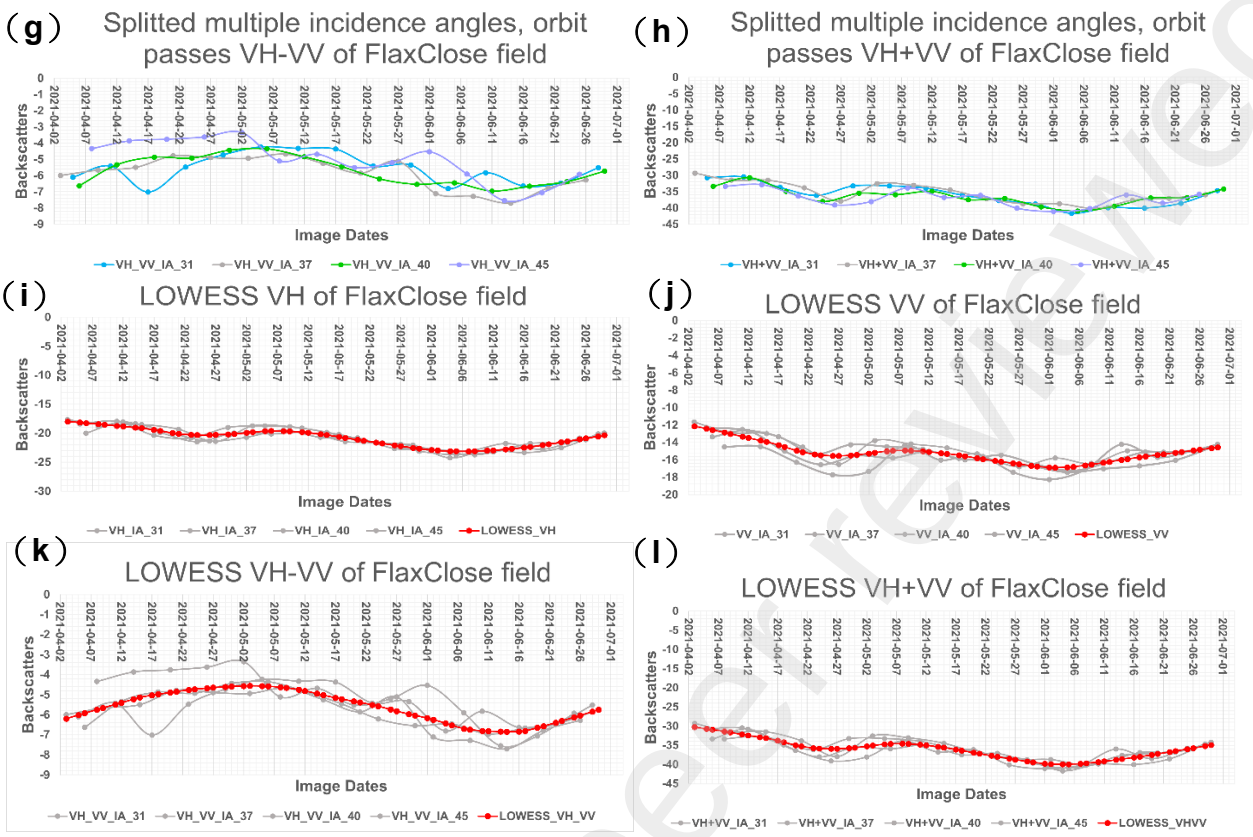

Fig. 3: The dense time series of backscatters for FlaxClose winter wheat fields in the UK. The backscatters (a) VH (b) VV (c) VH-VV (d)VH+VV of combined multiple incidence angles and orbit passes. The backscatters (e) VH (f) VV (g) VH-VV (h) VH+VV of splitted incidence angles 31°, 37°, 40°, 45° and orbit passes Ascending 30,103, Descending 52,154. The smoothen backscatters using LOWESS for (i) VH (j) VV (k) VH-VV (l) VH+VV.

3.2 Quantify backscatter parameters over plant traits using supervised machine learning algorithms.

The supervised machine learning models used were (1) Support Vector Machine (SVM) was originally developed to solve the classification problem (Cristianini & Shawe-Taylor, 2000) and then extended for solving regression problems. Support Vector Regression (SVR) can solve linear and nonlinear problems without changing predictor variables. It has been used for crop biophysical properties estimation (Yao et al., 2015; Kganyago et al., 2021). The best kernel configuration in this study was radial basis kernel function (RBF) in the R package. (2) Random Forest Regression (RFR) which is a widely used

non-linear regression using multiple decision trees for predicting the output (Breiman, 2001). RFR has been proven to be a useful exploratory and predictive tool for estimating crop properties (L. Wang et al., 2016; Mandal et al., 2019). In this study, we tuned the two parameters most likely to affect the final accuracy of the model, namely the number of randomly selected variables for each subset data point (*mtry)* and the number of trees to grow (*ntree).* Through `tuneGridRF`, we tuned *mtry* from 1 to 10 and selected the best *mtry* value based on the lowest RMSE. The default *ntree* = 500 has been applied in the model. (3) K-Nearest Neighbours Regression (KNNR) is another non-linear regression that is simple to implement (Baf et al., 2013). The algorithm is much faster than SVR and RF because it learns from the training dataset and makes real-time predictions when a new data point is added to the model. This algorithm has been advanced for the estimation of crop biophysical properties (Mansaray et al., 2020). These three machine learning approaches were optimized using 10-fold cross validation and the interaction depth at 3.

The processed VV, VH, VH-VV, and VH+VV backscatter parameters of Sentinel-1 were used as predictors, and the SD, GAI, AGDB, PH, and LNC as response variables. The VV, VH, VH-HV and VH+VV backscatter parameters for the five pixels aligned to the five sampling quadrats per field per visit were the input data for the supervised machine learning models. The robustness of the supervised machine learning models was evaluated in three scenarios, crop trait estimation models developed using (1) datasets in full growth stage (*Fig. 4)*, (2) datasets in growth stages indicative morphological change *(Fig. 5)* and (3) datasets in each principal growth stages (*Fig. 6*). These three scenarios not only evaluate the robustness of the machine learning algorithms, but also examine

the predictive power of Sentinel-1 backscatter parameter to crop traits in different time windows.

These models were validated by splitting the data into training and testing datasets with the ratio of ¾ and ¼ respectively. The training dataset was used to calibrate the three supervised machine learning models, whereas the testing dataset was used to investigate the performance and prediction power of the models. The coefficient of determination (R^2), root mean square errors (RMSE) and normalized root mean square error (NRMSE%) were computed to quantify the prediction power of the Sentinel-1 backscatter. The greatest R^2, smallest RMSE, and NRMSE closes to zero indicated good predictive model performance.

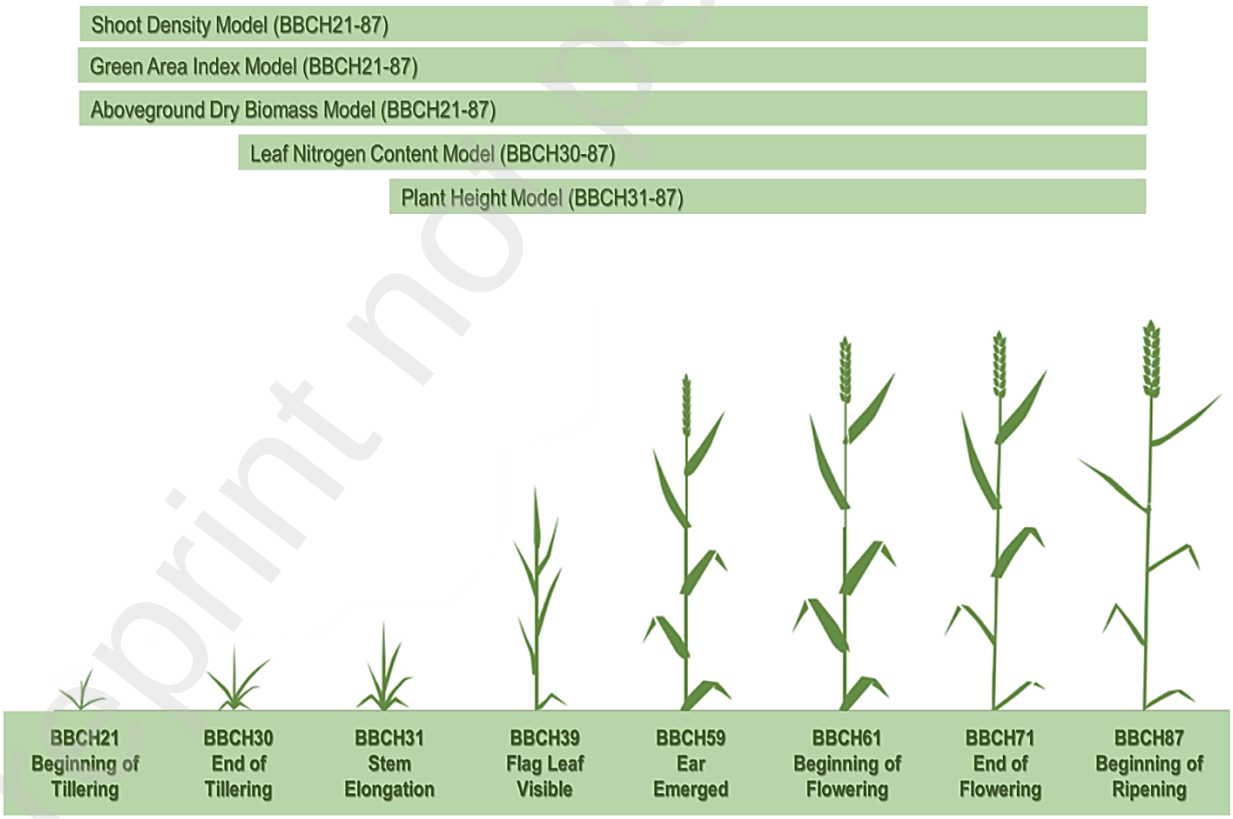

Fig. 4: Crop traits estimation models for full growth stages. Shoot density, green area index and aboveground dry biomass models were developed using data collected during BBCH21-87, leaf nitrogen content model using data collected during BBCH30-87 and plant height model using data collected during BBCH31-87.

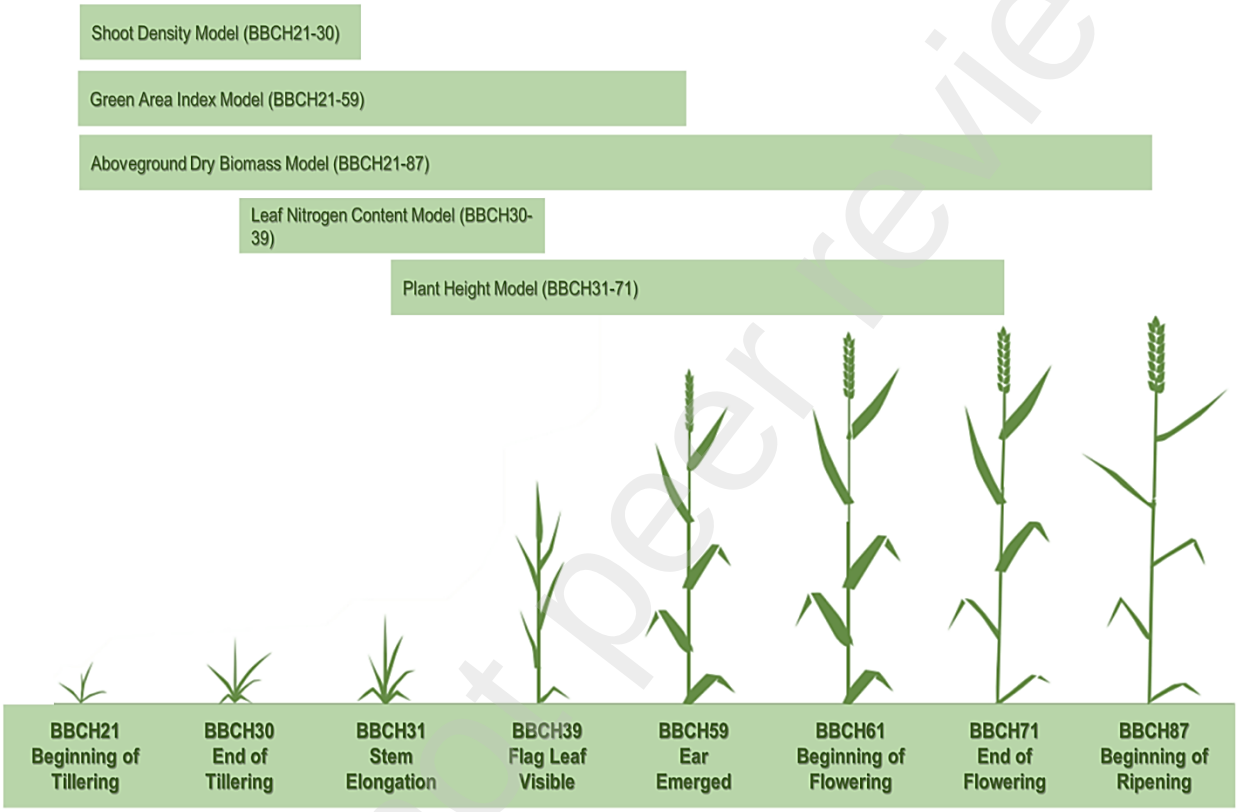

Fig. 5: Crop traits estimation models for specific growth stages indicative morphology change. Shoot density model was developed using data in BBCH21-30, green area index model in BBCH21-59, aboveground dry biomass model in BBCH21-87, leaf nitrogen content model in BBCH30-39 and plant height model in BBCH31-71.

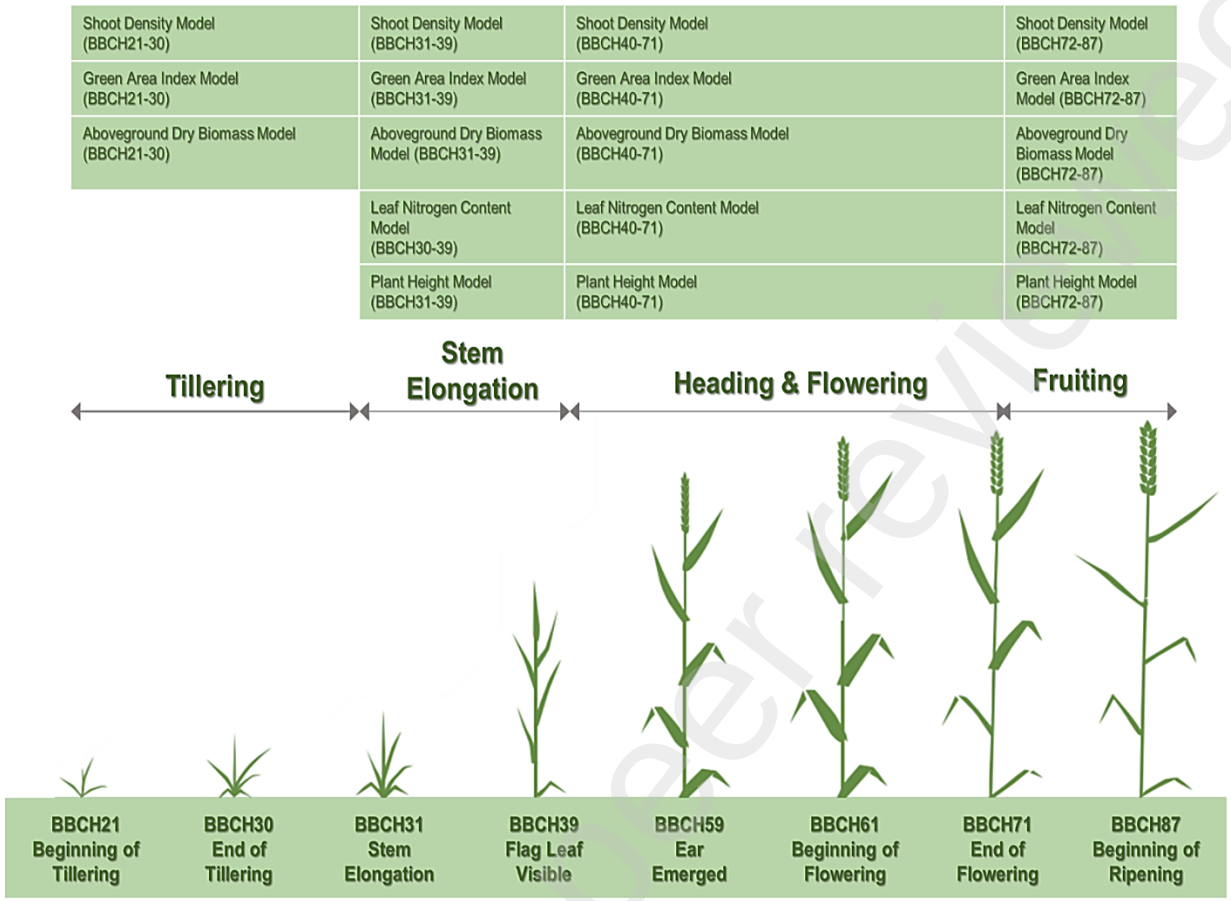

Fig. 6: Crop traits estimation models for each key growth stages, tillering (BBCH21-30), stem elongation (BBCH31-39), heading and flowering (BBCH40-71) and fruiting (BBCH72-87).

3.3 Trends in crop traits through the growing season

The trend of each in-situ plant trait during the growing season were evaluated to understand the morphological changes at different growth stages. The trends are useful as reference to determine the three scenarios (*Fig. 4*),(*Fig. 5) and (Fig. 6)* used to evaluate the supervised machine learning models. There was no change to the AGDB dataset because its morphology development started at BBCH21, beginning of tillering stage and continued throughout the full growth stages (*Fig. 9)*. The morphology

development of SD reduced after end of tillering at BBCH30 (*Fig. 7)*, GAI reached a maximum then stopped at ear emerged BBCH59 and declined thereafter (discussed below, presented in (*Fig. 8)*, PH developed while the stem was growing until the beginning of flowering stage BBCH61 and stagnated thereafter (*Fig. 10)*. The change of LNC increases from BBCH30-39 during the stem elongation and canopy expansion (*Fig. 11)*. Each crop trait will be considered in detail for developing the estimation models.

3.4 In-situ Shoot Density (SD)

The emergence of the side shoots at the leaf stem junction of winter wheat plant starts at BBCH21 and reaches its maximum after the end of tillering at BBCH30 (*Fig. 7*). The SD after BBCH30 varied from 613 shoots/m^2 to a maximum of 1500 shoots/m^2. The real-time assessment of SD per unit area could help to monitor winter wheat growth and yield (Tilley et al., 2019). Considering that each shoot can form a spike, it is an essential trait that could assist farmers in understand the management factors required to improve wheat yield (Bastos et al., 2020). After the stem elongation at BBCH31, SD decreases and fluctuates until ripening at BBCH87 *(Fig. 7).* The target final SD to achieve maximum potential yield in the UK is at least 460 shoots/m^2 (Sylvester-Bradley et al., 2018) and 480-600 shoots/m^2 in the IE (Lynch et al., 2016) by BBCH31.

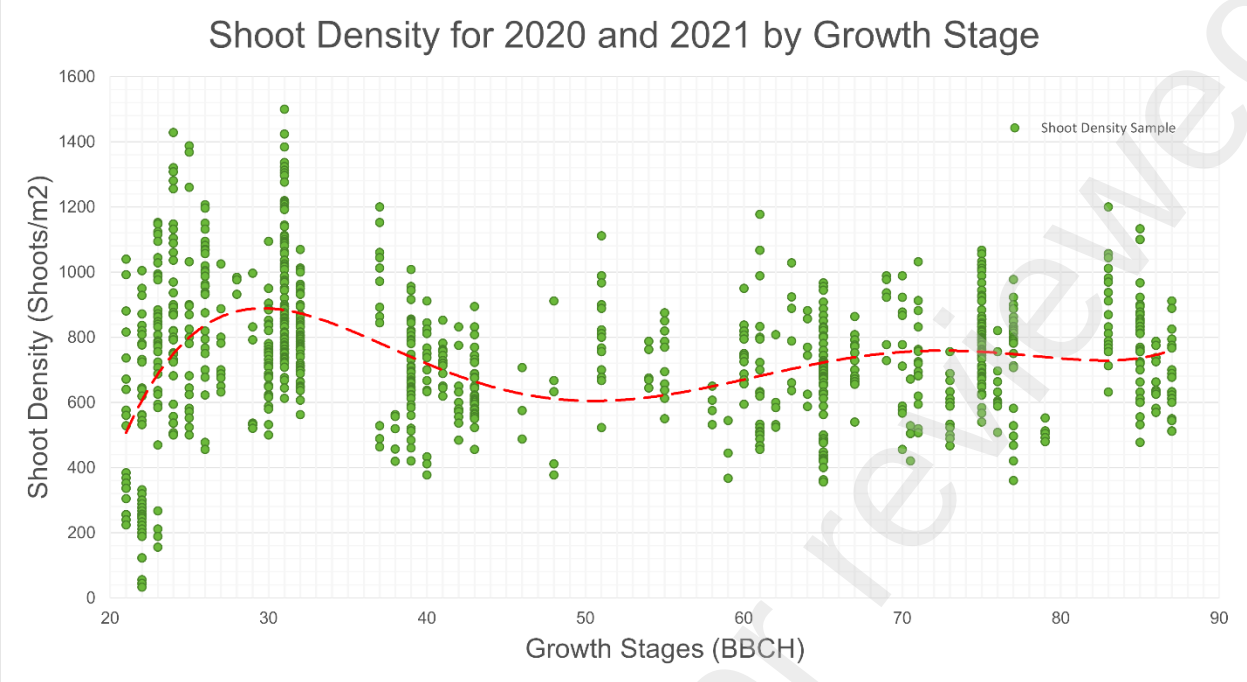

Fig. 7: The trend of observed winter wheat shoot density at different growth stages.

3.5 In-situ Green Area Index (GAI)

Crop canopy size is an essential crop variable that affects canopy photosynthesis capacity. To determine the radiation interception capacity of a crop, the canopy size is measured using GAI. GAI measured the total surface area of the green components of the canopy including leaves, stems, and ears divided by the ground surface area. Using real-time measurement of GAI, farmers can assess the crop condition and choose the optimal nitrogen management strategies for improved crop production (Sieling et al., 2013). It is apparent from the observed GAI in (*Fig. 8*), the canopy expansion of winter wheat begins at tillering BBCH21 and ends after the ear emerged at BBCH59. The GAI reaches a maximum of 8.00 m^2/m^2 to 8.4 m^2/m^2 at flag leaf visible BBCH39 to ear emerging at BBCH56 (*Fig. 8)*. If GAI declines during this period, it indicates a risk of foliar

disease (Bingham et al., 2009) or drought (Nezhadahmadi et al., 2013). Once the end of heading, the GAI starts to decrease as a result of leaves senescence. It is important to monitor the growth of GAI during BBCH21-59 to find out the effective amount and timing of fertilizer N applied and disease control measures and less important when GAI senesces from June onward which is after BBCH59.

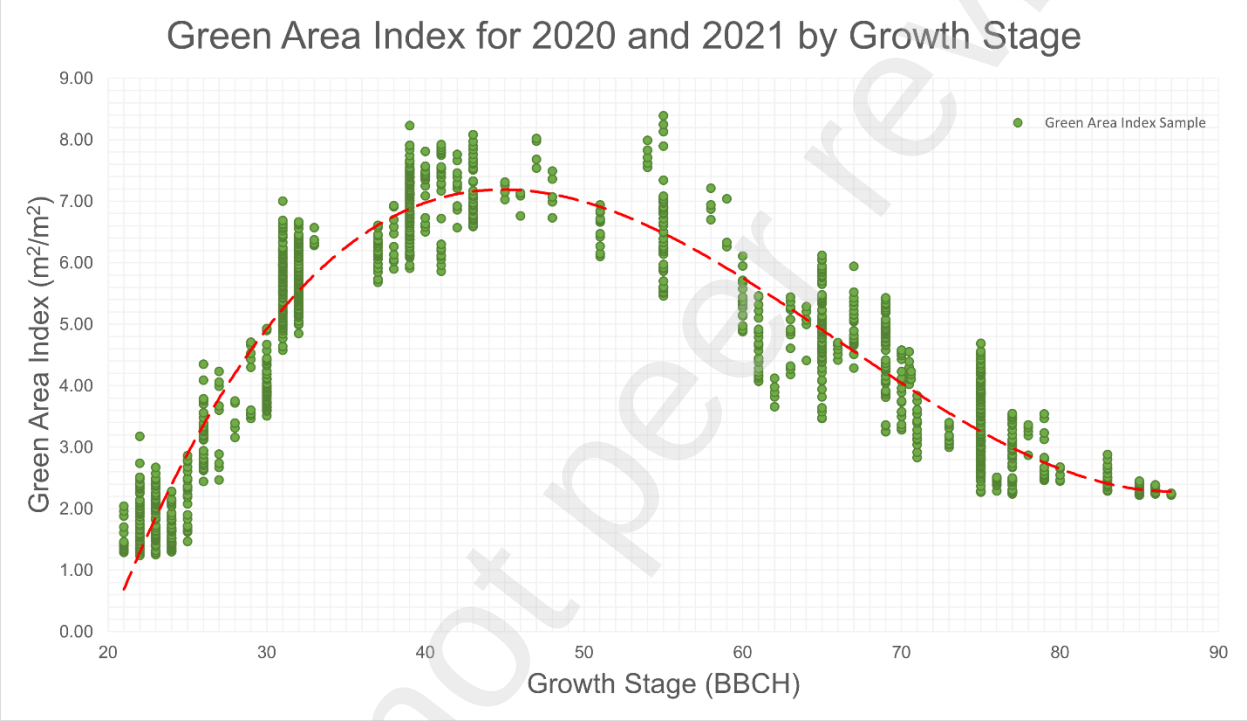

Fig. 8: The trend of observed winter wheat green area index at different growth stages

3.6 In-situ Aboveground Dry Biomass (AGDB)

Timely and accurate estimation of AGDB is another crucial component of crop health assessment, decision-making on optimal crop management strategies, and grain yield forecasts (Jaenisch et al., 2022). (*Fig. 9)* indicates how the observed wheat AGDB has changed over the growing season. Because of cold weather and low amounts of radiation

intercepted, AGDB is not significant prior to stem elongation before BBCH30. At stem elongation BBCH31, the AGDB begins to grow rapidly while the internode of wheat begins to extend. The stem contributes to most of the plant AGDB until the ear emerged at BBCH59. The AGDB shows an increasing trend with a higher rate than before from ear emerged BBCH59 to end of flowering BBCH71 as both stem and ear biomass accrue further together. At the end of flowering stage BBCH71, the stem biomass ceases and only grain accumulates AGDB, resulting in a peak AGDB level during early dough BBCH83. Subsequently, the accumulated AGDB then decreases from its maximum due to canopy senescence, leaf loss, and ongoing plant respiration (Lynch et al., 2016; Sylvester-Bradley et al., 2018).

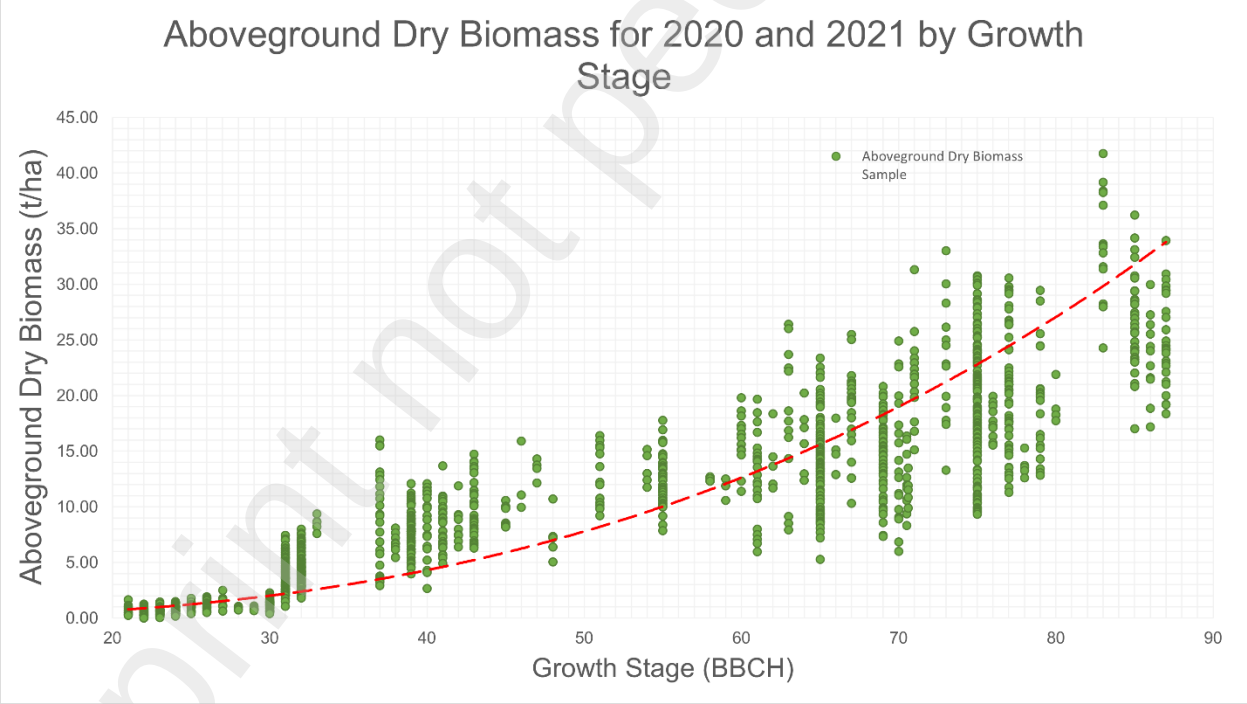

Fig. 9: The trend of observed winter wheat Aboveground Dry Biomass at different growth stages

3.7 In-situ Plant Height (PH)

PH is one of the predominant plant traits that affects wheat yield, morphological change, and lodging resistance (Y. Wang et al., 2017). Several studies found a significant negative correlation between wheat grain yield and PH (Islam et al., 2013; Gao et al., 2020). Taller wheat cultivars are more susceptible to lodging risk and a reduction in grain yield. PH is determined by the stem extension which begins at BBCH31. (*Fig. 10)* shows that the PH increases rapidly during the stem elongation and reaches a mean height of 64 cm at flag leaf visible BBCH39. After BBCH39, the PH increases at a gradual rate and reaches its final height between beginning of flowering at BBCH61 to end of flowering at BBCH71 in (*Fig. 10)*.

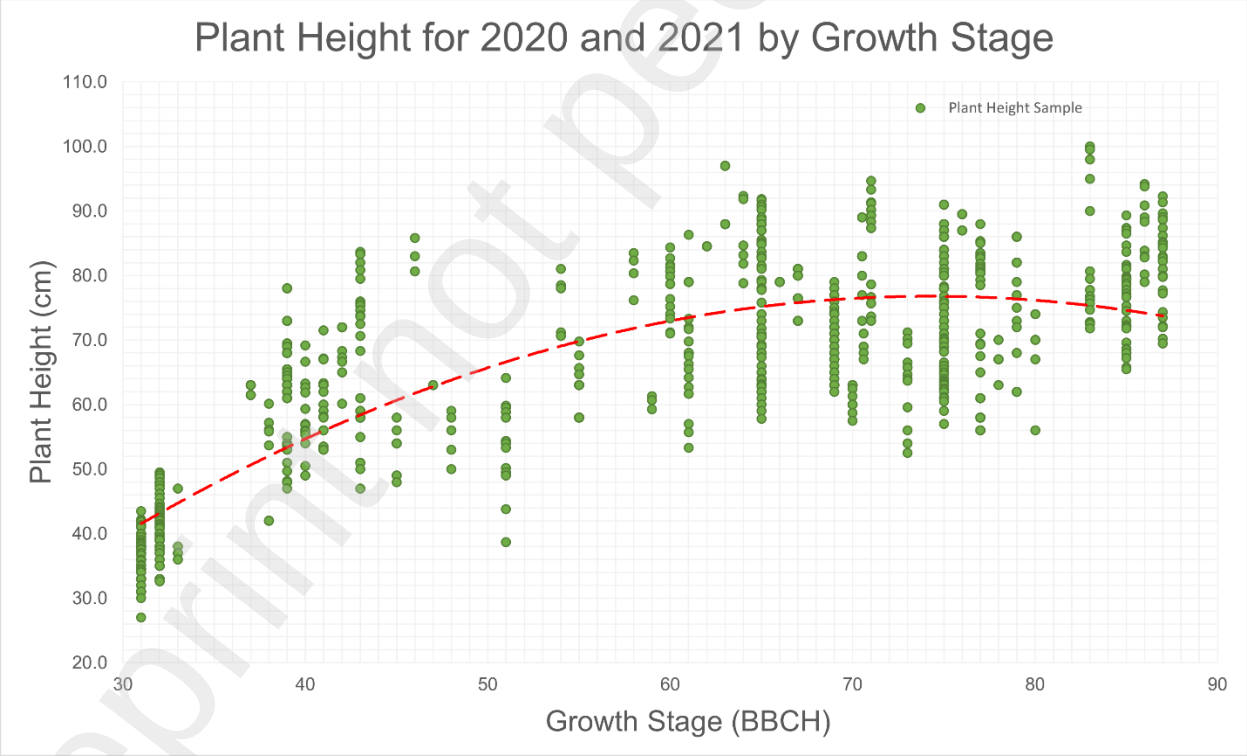

Fig. 10: The trend of observed winter wheat Plant Height at different growth stages

3.8 In-situ Leaf Nitrogen Content (LNC)

It is essential for a farmer to have a clear understanding of the nitrogen needs in wheat in order to apply nitrogen fertilizer more effectively (Spaner et al., 2005). The nitrogen content of leaves plays an important role in maintaining photosynthetic activity and nitrogen supply to the grain (Vilmus et al., 2014). (*Fig. 11)* illustrates the differences in observed LNC at different growth stages in the study area. Observed leaf nitrogen uptake begins at BBCH30, when stem elongation begins, and peaks at BBCH37, when flag leaf emerges. It has significant interaction in response to plant growth regulator accumulate split nitrogen applications at tillering BBCH21-26, stem elongation BBCH30-32 and flag leaf emerged BBCH37-39 (Qin et al., 2020; Peake et al., 2020). LNC begins to decline after BBCH51, which marks the beginning of heading. The declination of LNC can be explained by transfer of the photosynthesis assimilation substances to the head and ear (L. Wang et al., 2018).

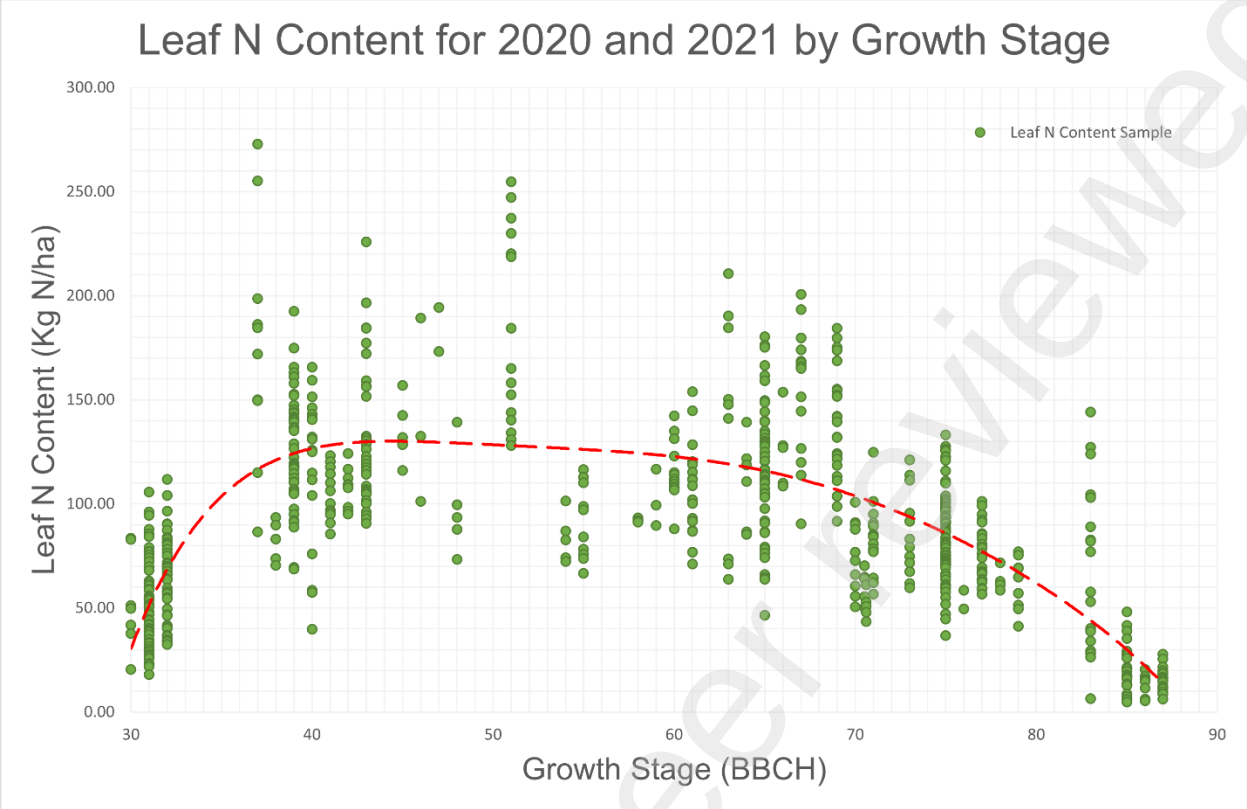

Fig. 11: The trend of observed winter wheat Leaf N Content at different growth stages.

4. Results

The analysis between the polarized backscatters parameters (VV, VH, VV-VH, and VV+VH) and each plant trait measurement (SD, GAI, AGDB, PH, and LNC) was conducted using supervised machine learning algorithms over full growth stages, plant morphological development stages, and key growth stage. The model's performance comparison results are shown in (*Table 3)*, (*Table 4)*, and (*Table 5)***.** The RFR models demonstrated the best prediction for both training and testing datasets of all the plant traits over the full growth stages (*Table 3*). The in-situ plant traits (SD, GAI, AGDB) were measured for full growth stages from BBCH21-BBCH87. However, measurements for PH

and LNC were available after the tillering and beginning of stem elongation at BBCH31 because no stems development and fully expanded leaves before this stage.

Among the plant traits, Sentinel-1 backscatter parameters have the greatest potential to estimate and predict GAI with all the algorithms. From the testing dataset, RFR had the best result for predicting GAI (R^2=0.94, RMSE=0.45m^2/m^2 and NRMSE=6%), followed by KNNR (R^2=0.94, RMSE=0.47m^2/m^2 and NRMSE=6%) and SVR (R^2=0.93, RMSE=0.50m^2/m^2 and NRMSE=6%). The result showed that Sentinel-1 backscatters had greater potential of estimating GAI than LAI (R^2=0.75) in Kumar et al., (2018). This finding also consistent with (Duveiller et al., 2011) that GAI is a more relevant plant trait due to satellite sensors' ability to capture reflectance and backscatter from changes in the canopy structure (Ulaby et al., 1986; Bouman & van Kasteren, 1990). AGDB has demonstrated good results as well as PH by using RFR for quantifying the potential of Sentinel-1 backscatters to estimate both plant traits with the performance of (R^2=0.87, RMSE=3.04 t/ha, and NRMSE=8%) and (R^2=0.85, RMSE=6.77 cm and NRMSE=10%) respectively. This study reported a higher accuracy of AGDB estimation using multivariate RFR model compared to univariate regression in the study of (Ferrazzoli et al., 1992) by using single HV polarized backscatter with R^2=0.75. Moreover, the result also showed a positive correlation between LNC and the backscatter parameters (R^2=0.69, RMSE=26.13 Kg N/ha, and NRMSE=10%). The backscatter parameters, on the other hand, exhibit the lowest prediction performance in SD (R^2=0.32, RMSE=165 shoots/m^2, and NRMSE=12%).

Table 3: Results of winter wheat plant traits estimation and prediction using Sentinel-1 backscatter parameters in training and testing datasets over full growth stages.

Plant Traits	Full Growth Stages	Machine Learning Models	Training Dataset			Testing Dataset		
			R^2	RMSE	NRMSE	R^2	RMSE	NRMSE
SD	BBCH21-87	SVR	0.21	188	0.13	0.24	175	0.13
(Shoots/m2)		***RFR***	***0.28***	***179***	***0.12***	***0.32***	***165***	***0.12***
		KNNR	0.27	181	0.12	0.32	166	0.13
GAI	BBCH21-87	SVR	0.93	0.52	0.06	0.93	0.50	0.06
(m2/m2)		***RFR***	***0.94***	***0.47***	***0.06***	***0.94***	***0.45***	***0.06***
		KNNR	0.94	0.49	0.06	0.94	0.47	0.06
AGDB	BBCH21-87	SVR	0.80	3.78	0.10	0.80	3.77	0.10
(t/ha)		***RFR***	***0.86***	***3.17***	***0.08***	***0.87***	***3.04***	***0.08***
		KNNR	0.84	3.36	0.09	0.86	3.17	0.08
PH	BBCH31-87	SVR	0.77	8.25	0.11	0.77	8.25	0.12
(cm)		***RFR***	***0.84***	***6.96***	***0.09***	***0.85***	***6.77***	***0.10***
		KNNR	0.82	7.30	0.10	0.83	7.02	0.10
LNC	BBCH30-87	SVR	0.60	28.87	0.11	0.62	29.31	0.12
(Kg N/ha)		***RFR***	***0.67***	***26.09***	***0.10***	***0.69***	***26.13***	***0.10***
		KNNR	0.65	26.85	0.10	0.69	26.43	0.11

The correlation between Sentinel-1 backscatters parameters and each plant trait measurement over its specific growth stage indicative the morphology development in plant is clearly shown in (*Table 4*). Based on results in (*Table 4)*, the prediction performance of SD, GAI, and PH using testing dataset had showcased better result than analysis using the full growth stages dataset in *(Table 3)*. The KNNR model showed equally good results as the RFR model in estimating the GAI. Same as the testing dataset,

the training dataset exhibited better prediction performance *(Table 4)* compares to dataset in full growth stages. However, the KNNR showed better results in estimating the SD than the RFR and SVR models. The overall performance ranking of supervised machine learning in this study is RFR>KNNR>SVR.

Table 4: Results of winter wheat plant traits estimation and prediction using Sentinel-1 polarized backscatters in training and testing dataset over morphology change stages.

Plant Traits	Morphology Development Stages	Machine learning models	Training Dataset			Testing Dataset		
			R^2	RMSE	NRMSE	R^2	RMSE	NRMSE
SD (Shoots/m^2)	BBCH21-30	SVR	0.28	239	0.18	0.31	217	0.17
		RFR	*0.28*	*238*	*0.18*	***0.33***	***211***	***0.17***
		KNNR	**0.29**	**236**	**0.18**	0.32	213	0.17
GAI (m^2/m^2)	BBCH21-59	SVR	0.95	0.47	0.07	0.95	0.47	0.07
		RFR	***0.95***	***0.46***	***0.06***	***0.95***	***0.46***	***0.06***
		KNNR	0.95	0.47	0.07	**0.95**	**0.46**	**0.06**
AGDB (t/ha)	BBCH21-87	SVR	0.80	3.78	0.10	0.80	3.77	0.10
		RFR	***0.86***	***3.17***	***0.08***	***0.87***	***3.04***	***0.08***
		KNNR	0.84	3.36	0.09	0.86	3.17	0.08
PH (cm)	BBCH31-71	SVR	0.78	6.65	0.11	0.78	6.68	0.13
		RFR	***0.87***	***6.08***	***0.08***	***0.87***	***5.96***	***0.09***
		KNNR	0.81	6.16	0.10	0.83	5.95	0.11
LNC (Kg N/ha)	BBCH31-39	SVR	0.64	25.85	0.14	0.66	27.08	0.16
		RFR	***0.73***	***25.57***	***0.10***	0.69	26.96	0.11
		KNNR	0.67	24.63	0.14	***0.71***	***24.31***	***0.14***

Further analysis of the correlation of Sentinel-1 backscatters parameters was conducted using the plant traits measurement over narrower time windows which are at each key growth stage namely tillering, stem elongation, heading & flowering, and fruiting. The results of (*Table 5)* indicate that, among the key growth stages, SD and GAI have the best prediction performance at tillering stage compared to other growth stages, while AGDB, PH, and LNC appear to have best prediction performance at the stem elongation stage. The best result of the plant trait model at the tillering stage is GAI with (R^2=0.85, RMSE=0.40m^2/m^2, NRMSE=11%). During stem elongation, PH exhibits the best prediction performance than the other plant traits (R^2=0.81, RMSE=5.24 cm, NRMSE=10%). GAI once again obtained the best prediction result among other plant traits at the heading and flowering stages with the result of (R^2=0.84, RMSE=0.53m^2/m^2, NRMSE=10%). The LNC with (R^2=0.71, RMSE=18.02 Kg N/ha, NRMSE=11%) has the best prediction result compared to others at fruiting stages. However, Sentinel-1 backscatter parameters had the best performance using datasets from growth stages indicative the morphology development of each plant traits than the datasets using the full growth stages and key growth stages respectively. This is due to insufficient representativeness of the ground truth sampling in a narrower time window for key growth stage.

Table 5: Results of winter wheat plant traits estimation and prediction using Sentinel-1 backscatter in training and testing datasets for key growth stages.

Plant Traits	Key Growth Stages	Machine learning models	Training Dataset			Testing Dataset		
			R^2	RMSE	NRMSE	R^2	RMSE	NRMSE
SD (Shoots/m^2)	***Tillering BBCH21-30***	***RFR***	*0.28*	*238*	*0.18*	***0.33***	***211***	***0.19***
	Stem Elongation BBCH31- 39	RFR	0.32	173	0.16	0.30	169	0.18
	Heading & Flowering BBCH40- 71	RFR	0.12	145	0.19	0.16	139	0.17
	Fruiting BBCH72- 87	RFR	0.27	133	0.17	0.31	129	0.18
GAI (m^2/m^2)	***Tillering BBCH21-30***	***RFR***	***0.86***	***0.39***	***0.11***	0.85	0.40	0.11
	Stem Elongation BBCH31- 39	RFR	0.59	0.46	0.13	0.58	0.45	0.12
	Heading & Flowering BBCH40- 71	RFR	0.83	0.53	0.10	0.84	0.53	0.10
	Fruiting BBCH72- 87	RFR	0.54	0.45	0.18	0.55	0.44	0.18
AGDB (t) /ha	Tillering BBCH21-30	RFR	0.39	0.37	0.15	0.45	0.35	0.17
	Stem Elongation BBCH31-39	***RFR***	0.52	1.85	0.12	***0.53***	***1.74***	***0.15***
	Heading & Flowering BBCH40- 71	RFR	0.45	3.40	0.12	0.45	3.33	0.15
	Fruiting BBCH72- 87	RFR	0.34	5.06	0.17	0.38	4.88	0.16
PH (cm)	***Stem Elongation BBCH31-39***	***RFR***	0.77	5.88	0.12	***0.81***	***5.24***	***0.10***
	Heading & Flowering BBCH40- 71	RFR	0.63	6.95	0.12	0.67	6.48	0.11

	Fruiting BBCH72- 87	RFR	0.25	8.75	0.18	0.28	8.51	0.18
LNC (Kg N/ha)	***Stem Elongation BBCH31-39***	***RFR***	***0.73***	***25.57***	***0.10***	0.69	26.96	0.11
	Heading & Flowering BBCH40- 71	RFR	0.37	30.54	0.14	0.52	27.79	0.13
	Fruiting BBCH72- 87	RFR	0.66	20.19	0.15	0.71	18.02	0.13

5. Discussions

5.1 Assessment of uncertainty for best performing models

The RFR algorithm provided the most accurate prediction models for plant traits in this study during the growth stages when the plant traits were developing and contributing to the morphological changes *(Table 4)*. (*Fig. 12)* shows the predicted versus observed plot of the winter wheat plant traits. The estimated SD for above 625 observed shoots/m^2 is close to the fitted line, the rest deviated from the fitted line making the model unsuitable for predicting the SD. This finding shows that Sentinel-1 backscatters have the greatest prediction power to GAI. The predicted GAI using the model distributed equally around the fitted line in (*Fig. 12b)*. AGDB is the second-best plant trait to have a good correlation with the Sentinel-1 backscatters. From the scatterplot in (*Fig. 12c)*, there are outliers around observed AGDB at 10-15 t/ha and 25-30 t/ha causing the prediction values to deviate from the fitted line. The estimated AGDB values are closer to the fitted line for the observed AGDB equal to or less than 10 t/ha. The PH RFR model demonstrated reliability to estimate the observed PH except for a few outliers caused overestimated values when

observed PH between 47-55 cm and underestimated when observed PH was above 77 cm. (*Fig. 12e)* illustrates RFR model overestimated observed LNC values between 100-125 Kg/ha.

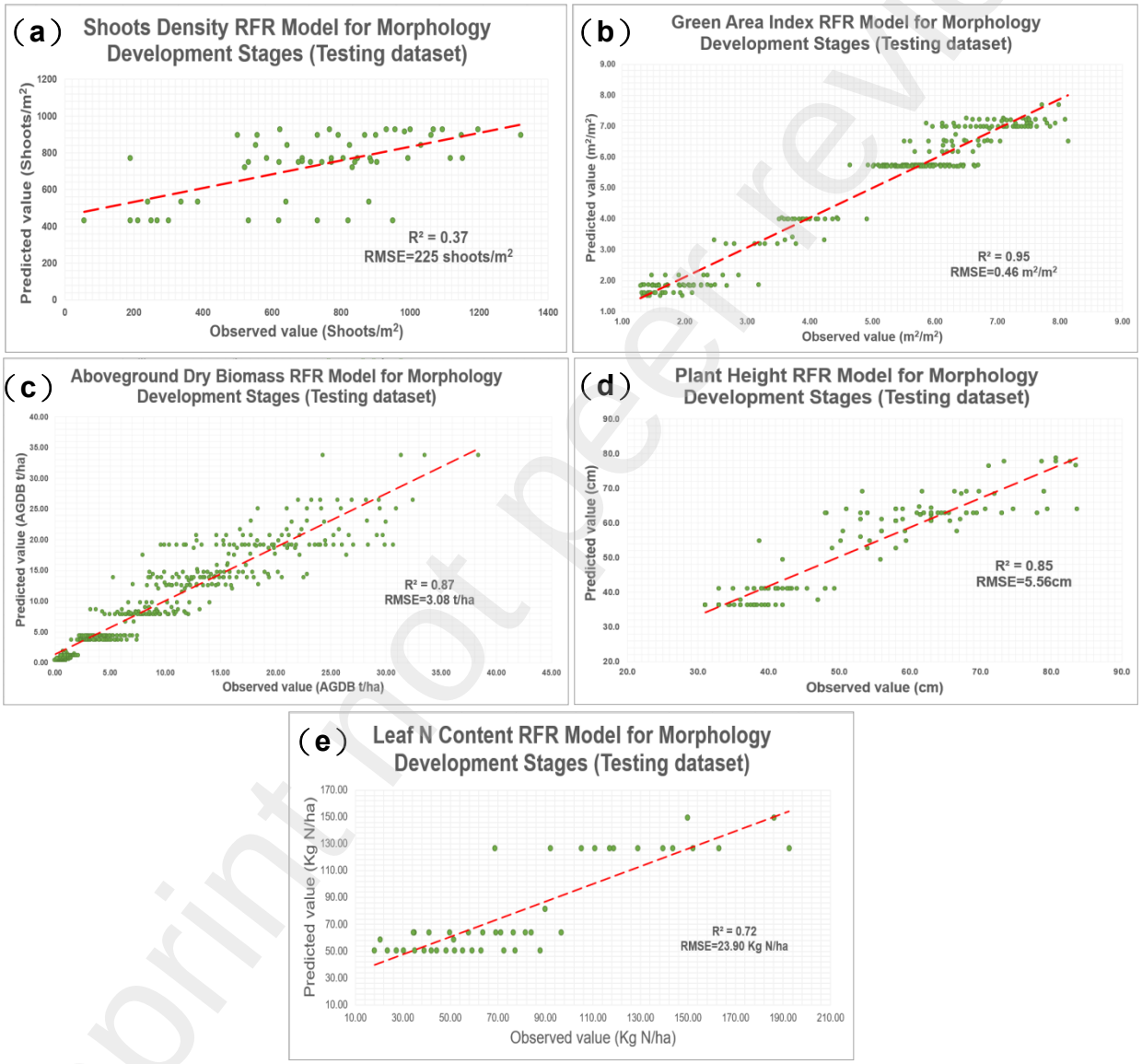

Fig. 12: The predictive performances of the RFR method for winter wheat plant trait estimations using Sentinel-1 backscatters in the testing datasets. (a)shoot density (SD), (b)green area index (GAI), (c) aboveground dry biomass (AGDB), (d)plant height (PH), (e) leaf nitrogen content (LNC). (R^2 indicates that the higher the prediction performance to the measured plant traits, the better the model).

5.2 Variable Importance of best performing models

RFR has a built-in variable importance function to identify the dependency of the crop traits estimation models to the Sentinel-1 backscatter parameters. The highest the importance value of the backscatter parameter, the highest contribution to the model performance. (*Fig.13a, c, e*) shows the cross-polarization ratio VH-VV has high contribution to the SD, AGDB, and LNC models. Many previous studies have also found significant correlations between VH-VV to winter wheat biophysical parameters (Vreugdenhil et al., 2018; Mercier et al., 2020; Nasirzadehdizaji et al., 2019) and high sensitivities to monitor phenological stages (Veloso et al., 2017; Schlund & Erasmi, 2020).

VH is the most influential Sentinel-1 backscatter parameter to the GAI estimation model (*Fig.13b*) but has no contribution to the SD estimation model. This is likely the result of volume scattering mechanisms of the crop. The study of Macelloni et al., (2001) also found that the VH increased with the increasing of LAI. Besides, Ferrazzoli et al., (1992) and (Paloscia et al., 1998) identified high correlation between VH and vegetation biomass of wheat. At low incidence angles, VH was most sensitive to the crop morphological change during crop development season (Moran et al., 2012).

VV is the only backscatter parameter that has influence on all the crop traits estimation models in this study. The influence of VV is primarily due to the change of the surface soil as the crop canopy decreased due to the increasing attenuation from the predominantly vertical structure of wheat stems (Nasrallah et al., 2019). The study of Brown et al. (2003) demonstrated that VV with high incidence angle around 40º contributed to monitoring fresh biomass, GAI, shoot number and growth stage of wheat.

The sum of VH+VV only shows significant contribution to estimate GAI and PH (*Fig.13*). The result is in contrast with Nasirzadehdizaji et al. (2019), where VH-VV (R^2=0.63) has slightly better correlation with PH compared to VH+VV (R^2=0.61). Gorrab et al. (2021) found that cumulative VH+VV improved estimation on PH to (R^2=0.89). Compared to VH-VV, VH+VV contributed the least or none to SD, AGDB and LNC estimation models.

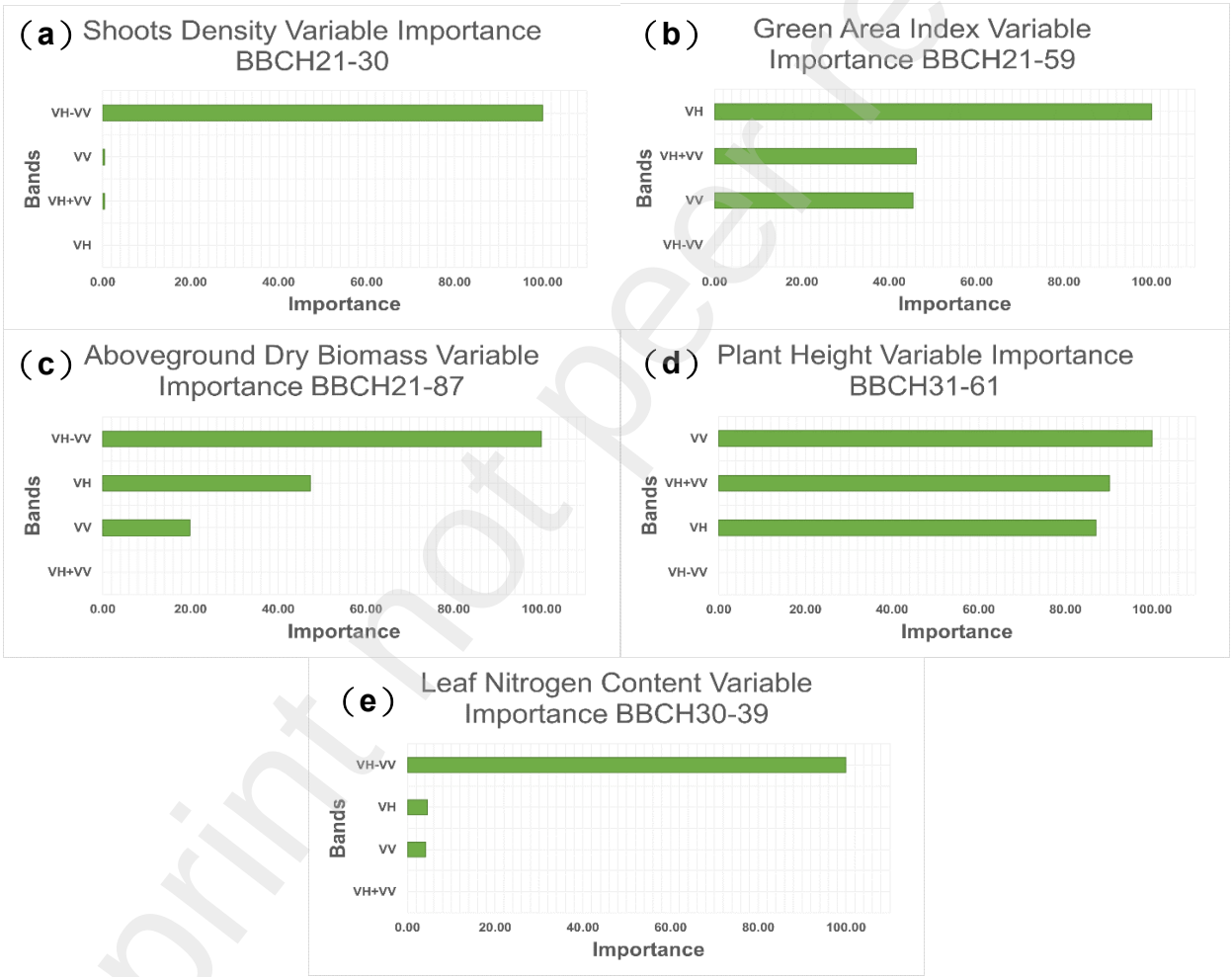

Fig.13: Important Sentinel-1 backscatters (ranked from high to low) for estimating (a) shoot density (SD), (b) green area Index (GAI), (c) aboveground dry biomass (AGDB), (d) plant height (PH), and (e) leaf nitrogen content (LNC).

5.3 Evaluation of results and outlooks

Based on our approach, the GAI estimation with multivariate machine learning using (VH, VV, VH-VV, and VH+VV) showed superior performance with (R^2=0.95 RMSE=0.46 m^2/m^2) over previous studies. For instance, Caballero et al., (2022) achieved (R^2=0.67 RMSE=0.88m^2/m^2) using VH+VV to estimate GAI. Harfenmeister et al., (2021a) applied combination of (VH, VV, VH/VV, Entropy, Anisotropy, and Alpha) to estimate LAI with (R^2=0.67). Our AGDB and PH estimation models had achieved the results of (R^2=0.87 RMSE=3.08 t/ha) and (R^2=0.87 RMSE=5.56 cm) respectively. Based upon the work performed in (Harfenmeister et al., 2021), their approach estimated dry biomass with (R^2=0.70) and plant height (R^2=0.76). As reported by Vreugdenhil et al. (2018), using univariate VH-VV has resulted to biomass estimation in (R^2=0.64), and crop height (R^2=0.68) of winter wheat. In Czech Republic, Tůma et al., (2022) demonstrated that using Radar Vegetation Index (RVI) for monitoring wheat canopy height (R^2=0.39). There was lack of information in previous literature of using Sentinel-1 backscatters to estimate SD and LNC. This research demonstrated improved performance in GAI, AGDB, PH, and LNC estimations except SD in winter wheat growth monitoring compared to existing work of (Goh et al., 2022) which was using Sentinel-2.

The analysis results help to understand the crop traits change from monitoring using the Sentinel-1 backscatter parameters. The accurate crop traits estimation model has great potential to create crop biophysical property maps which will be classified into informative crop management zone map at different phenology stages. Farmers and agronomists will be able to understand the crop condition in real time through the spatial variation in crop

management zone map and identify the most appropriate schedule and amount of fertilizer and pesticides. Ideally, the optimum nitrogen use efficiency requires matching fertilizer input to growth potential (Lemaire et al., 2008). The plant protection products should be sprayed with knowledge of the crop condition and disease intensity to gain positive net return (Wiik & Rosenqvist, 2010).

6. Conclusion

This study demonstrated the capability of C-Band Sentinel-1A/1B images with different incidence angles, various orbit directions (ascending and descending) and nine orbit passes to monitor winter wheat in a wide geographical extent covering IE and UK. This method can estimate the crop traits in wheat frequently and non-destructively at sub-field level. Based on our result, the RFR models clearly outperformed SVM and KNNR to quantify the correlation of Sentinel-1 backscatters to winter wheat plant trait due to its advantages of not sensitive to noise and collinearity (Cutler et al., 2007). However, it took longer training period than the other two algorithms. There were three scenarios we used (1) full phenology datasets, (2) morphology development stages, and (3) at each principal growth stage namely tillering, stem elongation, heading & flowering, and fruiting. To our knowledge, no study has considered evaluating the correlation of backscatters parameter to plant traits over different time windows during crop development. This could involve high expenditure and labor-intensive field sampling. The results suggested that the second scenario is most accurate in estimating the winter wheat plant trait change during the crop development using Sentinel-1 backscatter parameters. The sensitivity of Sentinel-1 backscatter parameters driven by phenological plant structural changes

(Vreugdenhil et al., 2018). The methodology framework of this study performed well even under different crop managements, soil types, climates, growing seasons, regions (IE and UK), and fertilizer rates. Therefore, it is possible that this methodology framework could be transferable to different agriculture regions. In future, this is essential for producing satellite-based crop trait performance variation maps to support the variable rate application and spray application technology in precision agriculture. Besides, the combination of crop traits performance can provide reliable insight to advance in-field yield performance forecast as early as during tillering stages.

CRediT author statement

B.B.Goh: Conceptualization, Methodology, Software, Validation, Formal analysis, Investigation, Data curation, Writing-original draft. **N.M.Holden:** Conceptualization, Investigation, Writing-review & editing, Supervision, Funding acquisition. **C.J. Bleakley**: Writing-review & editing. **S.Z.Sattari:** Writing-review & editing.

Acknowledgement

This research has been undertaken as part of the strategic partnership program between Science Foundation Ireland and ORIGIN Enterprises Limited, CONSUS funded under Grant Number 16/SPP/3296.

References

Anderson, K., & Croft, H. (2009). Remote sensing of soil surface properties. *Progress in Physical Geography: Earth and Environment*, *33*(4), 457–473. https://doi.org/10.1177/0309133309346644

Arias, M., Campo-Bescós, M. Á., & Álvarez-Mozos, J. (2022). On the influence of acquisition geometry in backscatter time series over wheat. *International Journal of Applied Earth Observation and Geoinformation*, *106*, 102671. https://doi.org/10.1016/j.jag.2021.102671

Atzberger, C. (2013). Advances in Remote Sensing of Agriculture: Context Description, Existing Operational Monitoring Systems and Major Information Needs. *Remote Sensing*, *5*(2), 949–981. https://doi.org/10.3390/rs5020949

Baf, S., Im, E., & Bol, M. (2013). *RESEARCH ARTICLE OPEN ACCESS Application of K-Nearest Neighbor (KNN) Approach for Predicting Economic Events: Theoretical Background*.

Baghdadi, N., Bazzi, H., El Hajj, M., & Zribi, M. (2018). Detection of Frozen Soil Using Sentinel-1 SAR Data. *Remote Sensing*, *10*(8), 1182. https://doi.org/10.3390/rs10081182

Bano, C., Amist, N., & Singh, N. B. (2019). Morphological and Anatomical Modifications of Plants for Environmental Stresses. In A. Roychoudhury & D. Tripathi (Eds.), *Molecular Plant Abiotic Stress* (1st ed., pp. 29–44). Wiley. https://doi.org/10.1002/9781119463665.ch2

Bastos, L. M., Carciochi, W., Lollato, R. P., Jaenisch, B. R., Rezende, C. R., Schwalbert, R., Vara Prasad, P. V., Zhang, G., Fritz, A. K., Foster, C., Wright, Y., Young, S., Bradley, P., & Ciampitti, I. A. (2020). Winter Wheat Yield Response to Plant Density as a Function of Yield Environment and Tillering Potential: A Review and Field Studies. *Frontiers in Plant Science*, *11*, 54. https://doi.org/10.3389/fpls.2020.00054

Bingham, I. J., Walters, D. R., Foulkes, M. J., & Paveley, N. D. (2009). Crop traits and the tolerance of wheat and barley to foliar disease. *Annals of Applied Biology*, *154*(2), 159–173. https://doi.org/10.1111/j.1744-7348.2008.00291.x

Bouman, B. A. M., & van Kasteren, H. W. J. (1990). Ground-based X-band (3-cm wave) radar backscattering of agricultural crops. II. Wheat, barley, and oats; the impact of canopy structure. *Remote Sensing of Environment*, *34*(2), 107–119. https://doi.org/10.1016/0034-4257(90)90102-R

Breiman, L. (2001). Random Forests. *Machine Learning*, *45*(1), 5–32. https://doi.org/10.1023/A:1010933404324

Brown, S. C. M., Quegan, S., Morrison, K., Bennett, J. C., & Cookmartin, G. (2003). High-resolution measurements of scattering in wheat canopies-implications for crop parameter retrieval. *IEEE Transactions on Geoscience and Remote Sensing*, *41*(7), 1602–1610. https://doi.org/10.1109/TGRS.2003.814132

Caballero, G., Pezzola, A., Winschel, C., Casella, A., Sanchez Angonova, P., Orden, L., Berger, K., Verrelst, J., & Delegido, J. (2022). Quantifying Irrigated Winter Wheat LAI in Argentina Using Multiple Sentinel-1 Incidence Angles. *Remote Sensing*, *14*(22), 5867. https://doi.org/10.3390/rs14225867

Cleveland, W. S. (1979). Robust Locally Weighted Regression and Smoothing Scatterplots. *Journal of the American Statistical Association*, *74*(368), 829–836. https://doi.org/10.1080/01621459.1979.10481038

Cristianini, N., & Shawe-Taylor, J. (2000). *An Introduction to Support Vector Machines and Other Kernel-based Learning Methods* (1st ed.). Cambridge University Press. https://doi.org/10.1017/CBO9780511801389

Cutler, D. R., Edwards, T. C., Beard, K. H., Cutler, A., Hess, K. T., Gibson, J., & Lawler, J. J. (2007). RANDOM FORESTS FOR CLASSIFICATION IN ECOLOGY. *Ecology*, *88*(11), 2783–2792. https://doi.org/10.1890/07-0539.1

Derkacheva, A., Mouginot, J., Millan, R., Maier, N., & Gillet-Chaulet, F. (2020). Data Reduction Using Statistical and Regression Approaches for Ice Velocity Derived by Landsat-8,

Sentinel-1 and Sentinel-2. *Remote Sensing*, *12*(12), 1935. https://doi.org/10.3390/rs12121935

Duveiller, G., Weiss, M., Baret, F., & Defourny, P. (2011). Retrieving wheat Green Area Index during the growing season from optical time series measurements based on neural network radiative transfer inversion. *Remote Sensing of Environment*, *115*(3), 887–896. https://doi.org/10.1016/j.rse.2010.11.016

Ferrazzoli, P., Paloscia, S., Pampaloni, P., Schiavon, G., Solimini, D., & Coppo, P. (1992). Sensitivity of microwave measurements to vegetation biomass and soil moisture content: A case study. *IEEE Transactions on Geoscience and Remote Sensing*, *30*(4), 750–756. https://doi.org/10.1109/36.158869

Gao, Z., Wang, Y., Tian, G., Zhao, Y., Li, C., Cao, Q., Han, R., Shi, Z., & He, M. (2020). Plant height and its relationship with yield in wheat under different irrigation regime. *Irrigation Science*, *38*(4), 365–371. https://doi.org/10.1007/s00271-020-00678-z

Goh, B.-B., King, P., Whetton, R. L., Sattari, S. Z., & Holden, N. M. (2022). Monitoring winter wheat growth performance at sub-field scale using multitemporal Sentinel-2 imagery. *International Journal of Applied Earth Observation and Geoinformation*, *115*, 103124. https://doi.org/10.1016/j.jag.2022.103124

Gorrab, A., Ameline, M., Albergel, C., & Baup, F. (2021). Use of Sentinel-1 Multi-Configuration and Multi-Temporal Series for Monitoring Parameters of Winter Wheat. *Remote Sensing*, *13*(4), 553. https://doi.org/10.3390/rs13040553

Han, D., Liu, S., Du, Y., Xie, X., Fan, L., Lei, L., Li, Z., Yang, H., & Yang, G. (2019). Crop Water Content of Winter Wheat Revealed with Sentinel-1 and Sentinel-2 Imagery. *Sensors*, *19*(18), 4013. https://doi.org/10.3390/s19184013

Harfenmeister, K., Itzerott, S., Weltzien, C., & Spengler, D. (2021). Agricultural Monitoring Using Polarimetric Decomposition Parameters of Sentinel-1 Data. *Remote Sensing*, *13*(4), 575. https://doi.org/10.3390/rs13040575

Islam, M. A., Obour, A. K., Saha, M. C., Nachtman, J. J., Cecil, W. K., & Baumgartner, R. E. (2013). Grain Yield, Forage Yield, and Nutritive Value of Dual-Purpose Small Grains in the Central High Plains of the USA. *Crop Management*, *12*(1), 1–8. https://doi.org/10.1094/CM-2012-0154-RS

Jaenisch, B. R., Munaro, L. B., Jagadish, S. V. K., & Lollato, R. P. (2022). Modulation of Wheat Yield Components in Response to Management Intensification to Reduce Yield Gaps. *Frontiers in Plant Science*, *13*, 772232. https://doi.org/10.3389/fpls.2022.772232

Kaplan, G., Fine, L., Lukyanov, V., Manivasagam, V. S., Tanny, J., & Rozenstein, O. (2021). Normalizing the Local Incidence Angle in Sentinel-1 Imagery to Improve Leaf Area Index, Vegetation Height, and Crop Coefficient Estimations. *Land*, *10*(7), 680. https://doi.org/10.3390/land10070680

Kganyago, M., Mhangara, P., & Adjorlolo, C. (2021). Estimating Crop Biophysical Parameters Using Machine Learning Algorithms and Sentinel-2 Imagery. *Remote Sensing*, *13*(21), 4314. https://doi.org/10.3390/rs13214314

Khabbazan, S., Vermunt, P., Steele-Dunne, S., Ratering Arntz, L., Marinetti, C., van der Valk, D., Iannini, L., Molijn, R., Westerdijk, K., & van der Sande, C. (2019). Crop Monitoring Using Sentinel-1 Data: A Case Study from The Netherlands. *Remote Sensing*, *11*(16), 1887. https://doi.org/10.3390/rs11161887

KONICA MINOLTA. (2009). *CHLOROPHYLL METER SPAD-502Plus*. 4.

Kumar, P., Prasad, R., Gupta, D. K., Mishra, V. N., Vishwakarma, A. K., Yadav, V. P., Bala, R., Choudhary, A., & Avtar, R. (2018). Estimation of winter wheat crop growth parameters using time series Sentinel-1A SAR data. *Geocarto International*, *33*(9), 942–956. https://doi.org/10.1080/10106049.2017.1316781

Lemaire, G., Jeuffroy, M.-H., & Gastal, F. (2008). Diagnosis tool for plant and crop N status in vegetative stage. *European Journal of Agronomy*, *28*(4), 614–624. https://doi.org/10.1016/j.eja.2008.01.005

Li, D., Wang, X., Zheng, H., Zhou, K., Yao, X., Tian, Y., Zhu, Y., Cao, W., & Cheng, T. (2018). Estimation of area- and mass-based leaf nitrogen contents of wheat and rice crops from water-removed spectra using continuous wavelet analysis. *Plant Methods*, *14*(1), 76. https://doi.org/10.1186/s13007-018-0344-1

Liu, C., Chen, Z., Shao, Y., Chen, J., Hasi, T., & Pan, H. (2019). Research advances of SAR remote sensing for agriculture applications: A review. *Journal of Integrative Agriculture*, *18*(3), 506–525. https://doi.org/10.1016/S2095-3119(18)62016-7

Lopez Laphitz, R. M., Ezcurra, C., & Vidal-Russell, R. (2016). Morphological Variation in <I>Quinchamalium</I> (Schoepfiaceae) is Associated with Climatic Patterns along its Andean Distribution. *Systematic Botany*, *40*(4), 1045–1052. https://doi.org/10.1600/036364415X690085

Lynch, J., Spink, J., Doyle, D., Hackett, R., Phelan, S., Forristal, D., Kildea, S., Glynn, L., Plunkett, M., Wall, D., Hutton, F., & Hennessy, M. (2016). *The Winter Wheat Guide*. Teagasc. https://www.teagasc.ie/media/website/publications/2016/Winter-Wheat-Guide.pdf

Macelloni, G., Paloscia, S., Pampaloni, P., Marliani, F., & Gai, M. (2001). The relationship between the backscattering coefficient and the biomass of narrow and broad leaf crops. *IEEE Transactions on Geoscience and Remote Sensing*, *39*(4), 873–884. https://doi.org/10.1109/36.917914

Mandal, D., Kumar, V., McNairn, H., Bhattacharya, A., & Rao, Y. S. (2019). Joint estimation of Plant Area Index (PAI) and wet biomass in wheat and soybean from C-band polarimetric SAR data. *International Journal of Applied Earth Observation and Geoinformation*, *79*, 24–34. https://doi.org/10.1016/j.jag.2019.02.007

Mansaray, L. R., Zhang, K., & Kanu, A. S. (2020). Dry biomass estimation of paddy rice with Sentinel-1A satellite data using machine learning regression algorithms. *Computers and Electronics in Agriculture*, *176*, 105674. https://doi.org/10.1016/j.compag.2020.105674

McDonald, K. C., Zimmermann, R., Way, J., & Chun, W. (1999). Automated instrumentation for continuous monitoring of the dielectric properties of woody vegetation: System design, implementation, and selected in situ measurements. *IEEE Transactions on Geoscience and Remote Sensing*, *37*(4), 1880–1894. https://doi.org/10.1109/36.774701

Meier, U., Bleiholder, H., Buhr, L., Feller, C., Hacks, H., Hess, M., Lancashire, P. D., Schnock, U., Stauss, R., Boom, T. van den, Weber, E., & Zwerger, P. (2009). The BBCH system to coding the phenological growth stages of plants—History and publications. *Journal Für Kulturpflanzen*, *61*(2), 41–52. https://www.cabdirect.org/cabdirect/abstract/20093092784

Mercier, A., Betbeder, J., Rapinel, S., Jegou, N., Baudry, J., & Hubert-Moy, L. (2020). Evaluation of Sentinel-1 and -2 time series for estimating LAI and biomass of wheat and rapeseed crop types. *Journal of Applied Remote Sensing*, *14*(02), 1. https://doi.org/10.1117/1.JRS.14.024512

Monsivais-Huertero, A., Judge, J., Liu, P.-W., & Chakrabarti, S. (2020). Monitoring Vegetation Conditions Over Agricultural Regions Using Active Observations. *IGARSS 2020 - 2020 IEEE International Geoscience and Remote Sensing Symposium*, 4351–4354. https://doi.org/10.1109/IGARSS39084.2020.9324414

Moran, M. S., Alonso, L., Moreno, J. F., Cendrero Mateo, M. P., de la Cruz, D. F., & Montoro, A. (2012). A RADARSAT-2 Quad-Polarized Time Series for Monitoring Crop and Soil Conditions in Barrax, Spain. *IEEE Transactions on Geoscience and Remote Sensing*, *50*(4), 1057–1070. https://doi.org/10.1109/TGRS.2011.2166080

Nasir, M., Ameen Ahmad, M., Hussain, S., & Ismaeel, M. (2019). Significance of Plant Growth Regulators (PGR's) on the Growth and Yield of Wheat Crop. *Science Journal of Chemistry*, *7*(5), 98. https://doi.org/10.11648/j.sjc.20190705.12

Nasirzadehdizaji, R., Balik Sanli, F., Abdikan, S., Cakir, Z., Sekertekin, A., & Ustuner, M. (2019). Sensitivity Analysis of Multi-Temporal Sentinel-1 SAR Parameters to Crop Height and Canopy Coverage. *Applied Sciences*, *9*(4), 655. https://doi.org/10.3390/app9040655

Nasrallah, A., Baghdadi, N., El Hajj, M., Darwish, T., Belhouchette, H., Faour, G., Darwich, S., & Mhawej, M. (2019). Sentinel-1 Data for Winter Wheat Phenology Monitoring and Mapping. *Remote Sensing*, *11*(19), 2228. https://doi.org/10.3390/rs11192228

Nezhadahmadi, A., Prodhan, Z. H., & Faruq, G. (2013). Drought Tolerance in Wheat. *The Scientific World Journal*, *2013*, 1–12. https://doi.org/10.1155/2013/610721

Ouaadi, N., Ezzahar, J., Khabba, S., Er-Raki, S., Chakir, A., Ait Hssaine, B., Le Dantec, V., Rafi, Z., Beaumont, A., Kasbani, M., & Jarlan, L. (2021). C-band radar data and in situ measurements for the monitoring of wheat crops in a semi-arid area (center of Morocco). *Earth System Science Data*, *13*(7), 3707–3731. https://doi.org/10.5194/essd-13-3707-2021

Paloscia, S., Macelloni, G., & Pampaloni, P. (1998). The relations between backscattering coefficient and biomass of narrow and wide leaf crops. *IGARSS '98. Sensing and Managing the Environment. 1998 IEEE International Geoscience and Remote Sensing. Symposium Proceedings. (Cat. No.98CH36174)*, 100–102 vol.1. https://doi.org/10.1109/IGARSS.1998.702811

Patel, P., & Srivastava, H. S. (2013). Ground Truth Planning For Synthetic Aperture Radar (SAR): Addressing Various Challenges Using Statistical Approach. *International Journal of Advancement in Remote Sensing, GIS and Geography*, *1*, 01–17.

Peake, A. S., Bell, K. L., Fischer, R. A., Gardner, M., Das, B. T., Poole, N., & Mumford, M. (2020). Cultivar × Management Interaction to Reduce Lodging and Improve Grain Yield of Irrigated Spring Wheat: Optimising Plant Growth Regulator Use, N Application Timing, Row Spacing and Sowing Date. *Frontiers in Plant Science*, *11*, 401. https://doi.org/10.3389/fpls.2020.00401

Qin, R., Noulas, C., Wysocki, D., Liang, X., Wang, G., & Lukas, S. (2020). Application of Plant Growth Regulators on Soft White Winter Wheat under Different Nitrogen Fertilizer

Scenarios in Irrigated Fields. *Agriculture*, *10*(7), 305. https://doi.org/10.3390/agriculture10070305

R Core Team. (2022). *R: A language and environment for statistical computing. R Foundation for Statistical Computing, Vienna, Austria.* https://www.R-project.org/

Schlund, M., & Erasmi, S. (2020). Sentinel-1 time series data for monitoring the phenology of winter wheat. *Remote Sensing of Environment*, *246*, 111814. https://doi.org/10.1016/j.rse.2020.111814

Schwerdt, M., Schmidt, K., Tous Ramon, N., Klenk, P., Yague-Martinez, N., Prats-Iraola, P., Zink, M., & Geudtner, D. (2017). Independent System Calibration of Sentinel-1B. *Remote Sensing*, *9*(6), 511. https://doi.org/10.3390/rs9060511

Sieling, K., Böttcher, U., & Kage, H. (2013). Growth stage specific optima for the green area index of winter wheat. *Field Crops Research*, *148*, 34–42. https://doi.org/10.1016/j.fcr.2013.04.002

Spaner, D., Todd, A. G., Navabi, A., McKenzie, D. B., & Goonewardene, L. A. (2005). Can Leaf Chlorophyll Measures at Differing Growth Stages be used as an Indicator of Winter Wheat and Spring Barley Nitrogen Requirements in Eastern Canada? *Journal of Agronomy and Crop Science*, *191*(5), 393–399. https://doi.org/10.1111/j.1439-037X.2005.00175.x

Sylvester-Bradley, R., Berry, P., Blake, J., Kindred, D., Spink, J., Bingham, I., McVittie, J., & Foulkes, J. (2018). *Wheat Growth Guide*. AHDB Cereals & Oilseeds. https://ahdb.org.uk/knowledge-library/wheat-growth-guide

Tilley, M. S., Heiniger, R. W., & Crozier, C. R. (2019). Tiller Initiation and its Effects on Yield and Yield Components in Winter Wheat. *Agronomy Journal*, *111*(3), 1323–1332. https://doi.org/10.2134/agronj2018.07.0469

Tůma, L., Kumhálová, J., Kumhála, F., & Krepl, V. (2022). The noise-reduction potential of Radar Vegetation Index for crop management in the Czech Republic. *Precision Agriculture*, *23*(2), 450–469. https://doi.org/10.1007/s11119-021-09844-5

Ulaby, F., Kouyate, F., Brisco, B., & Williams, T. H. (1986). Textural Information in SAR Images. *IEEE Transactions on Geoscience and Remote Sensing*, *GE-24*(2), 235–245. https://doi.org/10.1109/TGRS.1986.289643

Veloso, A., Mermoz, S., Bouvet, A., Le Toan, T., Planells, M., Dejoux, J.-F., & Ceschia, E. (2017). Understanding the temporal behavior of crops using Sentinel-1 and Sentinel-2-like data for agricultural applications. *Remote Sensing of Environment*, *199*, 415–426. https://doi.org/10.1016/j.rse.2017.07.015

Vilmus, I., Ecarnot, M., Verzelen, N., & Roumet, P. (2014). Monitoring Nitrogen Leaf Resorption Kinetics by Near-Infrared Spectroscopy during Grain Filling in Durum Wheat in Different Nitrogen Availability Conditions. *Crop Science*, *54*(1), 284–296. https://doi.org/10.2135/cropsci2013.02.0099

Voronov, S. I., Vlasova, O. I., Shtyrkhunov, V. D., Govorkova, S. B., & Savinov, E. V. (2021). The effect of growth regulators with retardant properties on the growth and development of winter wheat. *IOP Conference Series: Earth and Environmental Science*, *843*(1), 012022. https://doi.org/10.1088/1755-1315/843/1/012022

Vreugdenhil, M., Wagner, W., Bauer-Marschallinger, B., Pfeil, I., Teubner, I., Rüdiger, C., & Strauss, P. (2018). Sensitivity of Sentinel-1 Backscatter to Vegetation Dynamics: An Austrian Case Study. *Remote Sensing*, *10*(9), 1396. https://doi.org/10.3390/rs10091396

Wang, L., Sun, J., Wang, C., & Shangguan, Z. (2018). Leaf photosynthetic function duration during yield formation of large-spike wheat in rainfed cropping systems. *PeerJ*, *6*, e5532. https://doi.org/10.7717/peerj.5532

Wang, L., Zhou, X., Zhu, X., Dong, Z., & Guo, W. (2016). Estimation of biomass in wheat using random forest regression algorithm and remote sensing data. *The Crop Journal*, *4*(3), 212–219. https://doi.org/10.1016/j.cj.2016.01.008

Wang, Y., Zhao, J., Lu, W., & Deng, D. (2017). Gibberellin in plant height control: Old player, new story. *Plant Cell Reports*, *36*(3), 391–398. https://doi.org/10.1007/s00299-017-2104-5

Wiik, L., & Rosenqvist, H. (2010). The economics of fungicide use in winter wheat in southern Sweden. *Crop Protection*, *29*(1), 11–19. https://doi.org/10.1016/j.cropro.2009.09.008

Yan, W., Yang, B., & Zhang, Y. (2018). Characterizing the C-band Backscattering of Winter-Wheat Canopy with a Microwave Radiative Transfer Model. *2018 7th International Conference on Agro-Geoinformatics (Agro-Geoinformatics)*, 439–444. https://www.webofscience.com/wos/woscc/full-record/WOS:000468823900092

Yao, X., Huang, Y., Shang, G., Zhou, C., Cheng, T., Tian, Y., Cao, W., & Zhu, Y. (2015). Evaluation of Six Algorithms to Monitor Wheat Leaf Nitrogen Concentration. *Remote Sensing*, *7*(11), 14939–14966. https://doi.org/10.3390/rs71114939

Zhang, Y., Wu, T., Zhang, X., Sun, Y., Wang, Y., Li, S., Li, X., Zhong, K., Yan, Z., Xu, D., & Yao, J. (2022). Rayleigh Lidar Signal Denoising Method Combined with WT, EEMD and LOWESS to Improve Retrieval Accuracy. *Remote Sensing*, *14*(14), 3270. https://doi.org/10.3390/rs14143270